

1 **Abstract**

2 The Southern Ocean is known as the largest High-Nutrient, Low-Chlorophyll (HNLC) region
3 of the global ocean due to iron limitation. However, a large phytoplankton bloom develops
4 annually downstream of the Kerguelen Islands, a bloom which is sustained partly by iron
5 released from the sediments deposited onto the shelves. In the framework of the KEOPS-2
6 project, we used radium isotopes (^{224}Ra , $T_{1/2} = 3.66$ d; ^{223}Ra , $T_{1/2} = 11.4$ d; ^{228}Ra , $T_{1/2} = 5.75$ y)
7 to provide information on the origin of iron fertilization and on the timescales of the transfer
8 of sediment-derived inputs (including iron and other micronutrients) towards offshore waters.
9 Significant ^{224}Ra and ^{223}Ra activities were found in the near vicinity of the Kerguelen Islands,
10 in agreement with the short half-lives of these isotopes. Significant ^{224}Ra and ^{223}Ra activities
11 were also detected up to 200 km downstream of the islands and more unexpectedly in
12 offshore waters south of the Polar Front. These observations thus clearly indicate i) that the
13 sediment-derived inputs are rapidly transferred towards offshore waters (on timescales in the
14 order of several days up to several weeks) and ii) that the Polar Front is not a physical barrier
15 for the chemical elements released from the sediments of the Kerguelen Plateau. The Ra
16 dataset suggests that iron and other micronutrients released by the shelves of the Kerguelen
17 Islands may contribute to fuel the phytoplankton bloom downstream of the islands, despite the
18 presence of the Polar Front. However, the heterogeneous distribution of the ^{224}Ra and ^{223}Ra
19 activities in surface waters suggests that this supply across the front is not a continuous
20 process, but rather a process that is highly variable in space and time.

21

22 **Key words:** Southern Ocean, Iron fertilization, Radium isotopes, GEOTRACES

23 1 Introduction

24 The Southern Ocean is recognized as the major High-Nutrient, Low-Chlorophyll (HNLC)
25 region of the global ocean. Despite high nutrient concentrations, the phytoplankton growth
26 was shown to be limited by the very low iron concentrations in surface waters of the Southern
27 Ocean (De Baar et al., 1995; Martin et al., 1990). Dissolved iron is, however, supplied to the
28 surface waters in several locations of the Southern Ocean where iron is released by the shelf
29 sediments but this natural iron fertilization remains spatially limited (Tagliabue et al., 2014).
30 Consequently, high phytoplankton biomass can be found offshore the Antarctic continental
31 shelf (Arrigo et al., 2008; Moore and Abbott, 2002) or in the vicinity of subantarctic islands
32 (Blain et al., 2001; Korb et al., 2004; Pollard et al., 2007).

33 One of the largest phytoplankton blooms is observed offshore of the Kerguelen Islands,
34 in the Indian sector of the Southern Ocean (Blain et al., 2001). This phytoplankton bloom
35 extends more than 1000 km downstream of the Kerguelen Islands and shows two main
36 features: (i) a plume that extends northeastward of the islands and north of the Polar Front
37 (PF) that shows high mesoscale and temporal variability, and (ii) a larger bloom
38 southeastward of the islands and south of the PF (Blain et al., 2001, 2007). The two areas are
39 separated by a narrow band of relatively low chlorophyll concentration associated with the PF
40 that follows the inner shelf edge between 200 and 500 m isobaths (Park and Gamberoni,
41 1997; Park et al., 1998b). While Park et al. (2008a) suggest that the northward geostrophic
42 flow associated with the PF may possibly block any southward penetration of lithogenic
43 inputs released by the Kerguelen Islands, the numerous eddies and meanders formed along the
44 PF may contribute to transport chemical elements between the northern Kerguelen Plateau
45 and offshore waters.

46 The KEOPS-2 (Kerguelen ocean and plateau compared study) project aimed at
47 understanding the circulation patterns off the Kerguelen Islands and the mechanisms of iron
48 fertilization in that area. The KEOPS-2 cruise was conducted during austral spring 2011
49 eastward of the Kerguelen Islands. Natural radio-tracers such as radium isotopes (^{223}Ra , $T_{1/2} =$
50 11.4 d; ^{224}Ra , $T_{1/2} = 3.66$ d; ^{228}Ra , $T_{1/2} = 5.75$ y) have already been proved to be powerful tools
51 to track the origin and fate of chemical elements - including iron and other micronutrients -
52 that are released by the sediments deposited on the shelves (Annett et al., 2013; van Beek et
53 al., 2008; Charette et al., 2007; Dulaiova et al., 2009; Sanial et al., 2014). In this work, we
54 refer to these latter inputs as “sediment-derived inputs”. Radium isotopes are produced by the
55 decay of particle-bound thorium isotopes in the sediments and are delivered to the open ocean
56 by diffusion and advection processes. Thus, a water mass that interacts with shelf sediments is
57 potentially enriched in radium and in other elements that also diffuse out of the sediments
58 (e.g. iron, other micronutrients ...). While iron may then be removed from the water column
59 by biotic or abiotic processes, radium behaves as a conservative tracer. Radium is only
60 affected by radioactive decay and mixing in such a way that the water body keeps the
61 signature of its contact with the sediments. The radium signature of a given water mass may
62 then be transferred by diffusion and advection towards offshore waters. The presence of
63 significant Ra activities in offshore waters thus indicates that the water body has interacted
64 with shallow sediments. Alternatively, vertical mixing may also transport Ra towards surface
65 waters. Because radium isotopes decay, they can be used as chronometers to estimate the time
66 elapsed since the water body left the shelf, which in turn gives information on how quickly
67 the microelements released by the shallow sediments may be transferred to offshore waters
68 (Moore, 2000). In this work, we examined the distribution of ^{223}Ra , ^{224}Ra and ^{228}Ra in surface
69 waters downstream of the Kerguelen Islands in order (i) to investigate the origin and
70 dispersion of the sediment-derived inputs, including iron and (ii) to determine the apparent
71 ages of offshore waters that provide information on the timescales of the transfer of water and

72 associated chemical elements between the shelves and offshore waters. In addition to the Ra
73 distribution in surface waters, we report several vertical profiles of ^{223}Ra , ^{224}Ra and ^{228}Ra that
74 provide constraints on the vertical transport of chemical elements associated with vertical
75 mixing.

76 2 **Material and Methods**

77 2.1 The KEOPS-2 project

78 The KEOPS-2 cruise took place east of the Kerguelen Islands (northern Kerguelen
79 Plateau) between 14 October and 23 November 2011 on board the *R/V Marion Dufresne*
80 (IPEV: Institut Polaire Français – Paul Emile Victor and TAAF: Terres Australes et
81 Antarctiques Françaises). The KEOPS-2 project was designed to study the mechanisms of
82 natural iron fertilization downstream of the Kerguelen Islands and its impact on ecosystems
83 and biogeochemical cycles. The KEOPS-2 project was labelled as a GEOTRACES process
84 study and followed up a first KEOPS project conducted in 2005 in the area of the Southern
85 Kerguelen Plateau (Blain et al., 2007).

86 2.2 Study area

87 The Kerguelen Plateau, located in the Indian sector of the Southern Ocean, constitutes
88 one of the few physical barriers for the eastward-flowing Antarctic Circumpolar Current
89 (ACC). Various studies provide a detailed description of the general ocean circulation patterns
90 around the Kerguelen Plateau (Charrassin et al., 2004; Park and Gambéroni, 1995; Park et al.,
91 1998, 2008b, 2009). An important oceanographic feature of the area is the presence of the
92 Polar Front (PF), which is commonly characterized by the northernmost position of a
93 subsurface temperature minimum bounded by the 2 °C isotherm (Belkin and Gordon, 1996;
94 Park and Gamberoni, 1997; Park et al., 1993). A strong eastward current associated with this

95 front is deflected to the north at 71 °E following the eastern shelf slope of the Kerguelen
96 Plateau between the 200 and 500 m isobaths and forms a cyclonic meander that turns
97 southward at 75 °E (Belkin and Gordon, 1996; Orsi et al., 1995; Park and Gamberoni, 1997;
98 Park et al., 1993; Pollard et al., 2002). Numerous eddies are generated along the PF eastward
99 of the Kerguelen Plateau, that can, in some cases, be identified on the satellite composite
100 images of sea surface chlorophyll. The location of the stations investigated in this study is
101 shown on Fig. 1.

102 2.3 Radium data

103 2.3.1 Sample collection

104 Surface seawater samples were collected at 7 m depth using a clean pump specially
105 designed by IPEV for the KEOPS-2 cruise. Large volumes of surface seawater were collected
106 (250-900 L) and stored in large plastic tanks. We used a CTD (SBE-19plus, Seabird®) and a
107 rosette system equipped with 22x12-L Niskin bottles to collect seawater samples from various
108 depths throughout the water column. Three samples were also collected directly on two
109 beaches of the Kerguelen Islands (Baie du Morbihan: samples KER-1 and Baie des
110 Baleiniers: samples BaieB-1 and BaieB-2). Seawater samples were then passed by gravity
111 through PVC cartridges filled with “Mn-fibers” (MnO₂-impregnated acrylic fiber), following
112 (Moore, 2008). The flow rate was fixed at $\leq 0.5 \text{ L min}^{-1}$ to provide 100 % extraction
113 efficiency (Moore, 2008; van Beek et al., 2010). The Mn-fibers were then rinsed with MilliQ
114 water and partially dried before analysis.

115 2.3.2 Sample analysis

116 The Mn-fibers were analyzed using a Radium Delayed Coincidence Counter (RaDeCC;
117 (Charette et al., 2001; Moore and Arnold, 1996; Moore, 2008)). Three counting sessions are

118 necessary to determine both excess ^{224}Ra and excess ^{223}Ra activities in the samples. The first
119 counting was performed on board the research vessel during the cruise and provides the total
120 ^{224}Ra and ^{223}Ra activities. The Mn-fibers were analyzed again 3 weeks after sampling to
121 determine the ^{224}Ra activities supported by ^{228}Th and then after 3 months to determine the
122 ^{223}Ra activities supported by ^{227}Ac (Moore, 2000). The ^{224}Ra activities are corrected for the
123 ^{224}Ra supported by ^{228}Th and the ^{223}Ra activities are corrected for the ^{223}Ra supported by
124 ^{227}Ac . The ^{224}Ra and ^{223}Ra activities discussed hereafter thus refer to these excess ^{224}Ra and
125 ^{223}Ra activities. Uncertainties for both isotopes were calculated following Garcia-Solsona et
126 al. (2008) and were reported with one-sigma confidence interval.

127 Activities of ^{228}Ra were then determined using the low-background gamma detectors
128 placed at the LAFARA underground laboratory in the French Pyrénées (van Beek et al., 2010,
129 2013). Mn-fibers were either ashed at 820 °C for 16 h (Charette et al., 2001) and analyzed
130 using a well-type germanium detector or compressed and analyzed using a semi-planar
131 detector. Cross-calibrations between the two detectors were made to avoid any bias in the
132 determination of the Ra activities. Each sample was analyzed for ca. 120 hours to allow the
133 quantification of the low ^{228}Ra activities present in Southern Ocean waters (Kaufman et al.,
134 1973). ^{228}Ra activities were determined using ^{228}Ac peaks (338, 911 and 969 keV). All radium
135 activities are reported in disintegration per minute per 100 L of seawater (dpm/ 100 L). The
136 uncertainties reported for gamma counting consist in the error associated with counting
137 statistics (one sigma).

138 2.4 Physical data

139 2.4.1 Color data

140 High resolution maps ($1/25^\circ \times 1/25^\circ$) of chlorophyll concentration (mg/m^3) were
141 constructed by a 10-day weighted mean of MODIS and MERIS measurements. These satellite

142 products were delivered 3 times a week in near-real time during the cruise from Ssalto/Duacs
143 and CLS (Collecte Localisation Satellites, Toulouse, France) with support from CNES
144 (Centre National d'Etudes Spatiales, France). These images were used to define the sampling
145 strategy in the investigated area.

146 2.4.2 Surface drifters

147 Drifters provided by the US National Ocean and Atmospheric Administration
148 (NOAA) Global Drifter Program (GDP) were also released. The drogue is centered at 30 m
149 depth. These drifters thus provide information on the mean currents in the surface mixed layer
150 and on the dispersion of water masses due to eddy activities. Successive positions of the
151 drifter were transmitted to the R/V Marion Dufresne four times a day by the NOAA GDP
152 center. The time-irregular positions of the drifter were interpolated into a regular time step of
153 12 minutes and a low-pass filter of 48 hours was then applied to filter all tidal currents and
154 inertial oscillations.

155 2.4.3 Lagrangian particle analysis

156 The Lagrangian particle analysis was based on total surface currents, which are the sum
157 of the absolute geostrophic currents (deduced from altimeter product) and Ekman currents
158 (daily mean). The Ekman component is deduced from the European Centre for Medium-
159 Range Weather Forecasts (ECMWF) wind stress analysis applying a regional Ekman model,
160 specifically adjusted for the Kerguelen area. The altimeter current products were produced by
161 Ssalto/Duacs and distributed by AVISO, with support from CNES. Total surface currents
162 were delivered every day with a $1/8^\circ \times 1/8^\circ$ resolution. Details of the mapping technique are
163 given by Dibarboure et al. (2011).

164 2.4.4 Lagrangian Model

165 The altimetry-derived velocities providing the geostrophic mesoscale velocity at the
166 ocean surface were analyzed in near-real time with a Lagrangian model. This model was
167 inspired by Mongin et al. (2009) who reconstructed the extension of the Kerguelen
168 chlorophyll plume with a transport scheme based on altimetry. The model created thousands
169 of virtual surface drifters released on the shelf break of Kerguelen (2000 m isobaths; apparent
170 age = 0). The trajectories were constructed by backward-in-time integration of the altimetric
171 velocity field and were stopped when a hit over the Kerguelen shelf break was detected
172 (indicating a trajectory coming from the shelf), or when a maximum integration time—set to
173 120 days—was reached (indicating no interaction with the shelf on the past 120 days). This
174 model was applied successfully by Sanial et al. (2014) to highlight the key role played by
175 surface horizontal transport in defining the extension of the spring-time chlorophyll plume in
176 the Crozet area.

177 **3 Results**

178 3.1 Hydrological context during the KEOPS-2 cruise

179 The KEOPS-2 cruise lasted almost two months (October-November 2011). During that
180 period, the phytoplankton bloom developed off the Kerguelen Islands (Fig. 2). The satellite
181 composite images of sea surface chlorophyll reveal a complex shape of the phytoplankton
182 bloom that may be associated with the complex hydrography of the area. High concentration
183 of chlorophyll first appeared close to the Kerguelen Islands (October 2011) before spreading
184 out in offshore waters until covering a large part of the study area at the end of November
185 2011. East of the Kerguelen Islands, a narrow band of low chlorophyll concentration is
186 associated with the northward branch of the PF that splits the phytoplankton bloom into two
187 parts.

188 The PF also delimits two surface water masses characterized by a strong contrast in
189 temperature and salinity; the Antarctic Surface Water (AASW) is located south of the PF, and
190 the SubAntarctic Surface Water (SASW) is located north of the PF (Emery and Meincke,
191 1986). The potential temperature-salinity diagrams of the water masses investigated in this
192 study are shown in Fig. 3. The SASW is identified only at station F-L, suggesting that this
193 station is located north of the PF. The Winter Water (WW), a typical feature of the Antarctic
194 Zone that is characterized by a subsurface temperature minimum layer around 200 m depth
195 (Park et al., 1998a, 2008b, 2014) is found on all the vertical profiles reported here, except for
196 station F-L, thus confirming its location north of the PF. Below the WW, three water masses
197 can be identified: the Upper Circumpolar Deep Water (UCDW), the Lower Circumpolar Deep
198 Water (LCDW) and the Antarctic Bottom Water (AABW) (Park et al., 1993, 2008b). Note
199 that the AABW is only found on the F-L profile (commonly observed below 2600 m in this
200 area; (Park et al., 2008b)).

201 3.2 Radium distribution in surface waters

202 The radium activities reported in this study are shown in Table 1 and fall in the range
203 of previous radium data reported for surface waters near islands of the Southern Ocean
204 (Annett et al., 2013; Charette et al., 2007; Dulaiova et al., 2009; Hanfland, 2002; Kaufman et
205 al., 1973; Sanial et al., 2014; van Beek et al., 2008). The highest ^{223}Ra , ^{224}Ra and ^{228}Ra
206 activities are found in seawater samples collected at shallow stations near the Kerguelen
207 Islands (bathymetry < 200 m; Fig. 4). The radium activities then gradually decrease offshore.
208 Several samples, however, display significant ^{224}Ra activities in samples collected offshore
209 (Fig. 4a): stations UW-21-23-34 and TEW-7 located along the PF; stations UW-32, E-1 and
210 TEW-5 south of the PF; and station TNS-1 north of the PF. A greater number of offshore
211 stations exhibit significant ^{223}Ra activities, which agrees with the longer half-life of the ^{223}Ra
212 isotope (Fig. 4b). The stations displaying significant ^{224}Ra activities also display significant

213 ^{223}Ra activities. The radium activities are especially high at station TNS-2 located north of the
214 PF and at stations E-1 and G-1, located south of the PF. Station G-2 was visited twice and
215 showed high ^{223}Ra and ^{224}Ra activities at both visits. Station A3 located on the southern
216 Kerguelen Plateau was also visited twice. Significant ^{223}Ra and ^{224}Ra activities were
217 determined in the water sample collected at station A3-1 during the first visit at station A3
218 (note however that these activities are low) but were both below the detection limit at station
219 A3-2 (second visit at station A3). In contrast, the ^{228}Ra activities are similar at the two visits
220 of A3 (Table 1). All surface samples display significant ^{228}Ra activities up to ca. 300
221 kilometers offshore from the Kerguelen Islands (i.e. station TEW-8). Relatively high values
222 are observed at stations TNS-2 and UW-32 located north and south of the PF, respectively
223 (Fig. 4c). Station R-2, which was chosen as the reference station for typical HNLC waters east
224 of the Kerguelen Islands, shows significant ^{223}Ra , ^{224}Ra and ^{228}Ra activities in surface waters.

225 3.3 Vertical distribution of Ra isotopes

226 The study of the vertical distribution of Ra isotopes allows us to provide constraints on
227 the vertical transport of Ra associated with vertical mixing. Consequently, these profiles help
228 us to define the origin of the Ra enrichments observed in surface waters off the Kerguelen
229 Islands (lateral versus vertical supply of Ra). The major water masses, identified with the
230 potential temperature-salinity diagrams throughout the water column are reported for each
231 profile. The shallow Ra profiles (stations TEW-3, G-1 and A3-2) are shown on Fig. 5 and the
232 deep profiles (stations F-L, E-4W and E-1) are shown on Fig. 6.

233 The ^{223}Ra and ^{224}Ra activities are usually higher in samples collected near the seafloor
234 and are below the detection limit at intermediate depths (Table 2; Fig. 5 and 6). Significant
235 ^{223}Ra and ^{224}Ra activities are observed in surface and/or subsurface waters several kilometers
236 offshore from the islands, in particular at stations G-1 and E-1 located south of the PF and at

237 station F-L located north of the PF. The vertical profiles of ^{223}Ra and ^{224}Ra are quite unique at
238 station F-L. Although i) this station is located far from the Kerguelen Islands and ii) the
239 bottom is at 2670 m depth, the ^{223}Ra and ^{224}Ra activities are relatively high throughout the
240 water column (Fig. 6). Significant ^{228}Ra activities were found in the different water columns
241 investigated in this study. The ^{228}Ra activities at stations TEW-3 and G-1 are relatively high
242 and uniform throughout the water column. The ^{228}Ra activities at station A3 are uniform in
243 the upper 250 m and then increase with increasing water depth. The vertical ^{228}Ra profiles at
244 the deep stations (F-L, E-1 and E-4W) exhibit an increasing trend with increasing depth
245 reflecting the diffusion of radium out of the sediments. This latter pattern is also especially
246 marked at station A3 on the southern Kerguelen Plateau (Fig. 5).

247 **4. Discussion**

248 4.1 Origin of the radium enrichments in surface waters

249 The relatively high radium activities (^{223}Ra , ^{224}Ra and ^{228}Ra) observed in surface
250 waters east of the Kerguelen Islands may be explained either by the vertical transport or
251 diffusion that supplies radium to surface waters or by the lateral advection of waters that have
252 recently interacted with shallow sediments (Blain et al., 2001; Park et al., 2008a, van Beek et
253 al., 2008).

254 When considering solely the ^{228}Ra vertical profiles - that show in most cases an increase
255 of ^{228}Ra activities with increasing depth - it cannot be excluded that the vertical mixing
256 contributes to increase radium activities in surface waters. However, the ^{224}Ra and ^{223}Ra
257 vertical profiles – that show higher Ra activities in the upper and in the deep water column but
258 Ra activities below the detection limit in the mid water column - clearly indicate that the
259 higher ^{224}Ra and ^{223}Ra activities in surface waters cannot be explained by vertical mixing. The

260 ^{224}Ra and ^{223}Ra enrichments in surface waters are thus more likely explained by the lateral
261 advection of waters that have recently interacted with shallow sediments.

262 The northward advection of a water mass that has interacted with the shallow
263 sediments deposited on the shelves of Heard Island has been identified as a pathway for the
264 micronutrients that sustain the phytoplankton bloom on the southern Kerguelen Plateau
265 (Chever et al., 2010; van Beek et al., 2008; Zhang et al., 2008). The presence of a chlorophyll
266 plume that expands northward of the southern Kerguelen Plateau may also support the
267 existence of this northward advection (Fig. 2). The observation of significant ^{224}Ra and ^{223}Ra
268 activities in surface waters at station A3-1 confirms this circulation pattern and suggests that
269 the transit time of the waters that interacted with the shelves of Heard Island may be <1
270 month between Heard Islands and station A-3. This is in agreement with the Ra data obtained
271 in 2005 during the KEOPS-1 project, where significant ^{224}Ra and ^{223}Ra activities were also
272 found in surface waters at station A3 (van Beek et al., unpublished data). When the waters
273 move further north towards the area investigated in this study, the ^{224}Ra and ^{223}Ra activities
274 will then continue to decay. Two drifters released during the KEOPS-2 cruise at station A3
275 allow us to provide constraints on the transit time between the southern Kerguelen Plateau
276 and the studied area (eastward of Kerguelen at around 49 °S). A first drifter recirculated
277 around station A3 nearly 20 days before it moved slowly northward. It took approximately
278 60-75 days for the drifter to reach the investigated area located eastward of the Kerguelen
279 Islands (Fig. 7). It took approximately 53-65 days for the second drifter to reach the area
280 eastward of Kerguelen. Such transit times agree with the estimate of Park et al. (2008b)
281 during the KEOPS-1 project (i.e. several months between Heard Islands and the eastern flank
282 of the Kerguelen Islands). With such a transit time, a water body that interacted with the
283 shelves of Heard Island should not contain any remaining short-lived radium isotopes when
284 reaching the eastern flank of the Kerguelen Islands. As a consequence, the ^{224}Ra and ^{223}Ra

285 activities found in offshore waters east of the Kerguelen Islands, south of the PF are best
286 explained by diffusion or advection of Ra via waters that recently interacted with the shallow
287 sediments of the northern Kerguelen Plateau. This scenario, however, implies that the Ra
288 isotopes (and potentially other chemical elements such as iron) were transferred offshore
289 across or via the PF. High dissolved and particulate trace element concentrations (Fe, Ni and
290 Co) were also found east of the PF confirming that chemical elements may be transported
291 offshore across or via the PF (Qu  rou   et al. 2014; van der Merwe et al., 2014). Among the
292 potential mechanisms allowing surface waters to be transported eastward across the PF, one
293 can invoke either i) the wind stress (eastward winds are especially strong in that region) or ii)
294 eddies that form along the PF and that could promote the passage of chemical elements across
295 the front.

296 However, a contribution of surface waters originating from the southern Kerguelen
297 Plateau may not be completely excluded. In contrast to ^{224}Ra and ^{223}Ra that both disappear
298 due to radioactive decay along the northward transport, ^{228}Ra with a longer half-life would
299 remain in these waters. The ^{228}Ra activities observed eastward of the Kerguelen Islands may
300 thus be partly explained by an advective transport of waters originating from the south. It
301 cannot be excluded, therefore, that the northward advection originating from the southern
302 plateau contributes to the natural fertilization of the investigated area, in addition to the input
303 of chemical elements across the PF that was shown by the short lived isotopes.

304 South of the Kerguelen Islands (i.e. along the Polar Front at stations UW-23 and UW-24
305 or south of the Polar Front e.g. at stations UW-15, UW-16, R-2; Figure 4), it cannot be
306 completely excluded that the observed radium enrichments are partly explained by an input of
307 radium associated with the Leclaire Rise located west of the Kerguelen Islands at ca 350 m
308 depth (Weis and Frey, 2002). Station R-2, which is located east of the Leclaire Rise south of
309 the Polar Front, shows significant ^{223}Ra and ^{224}Ra activities in surface waters. Although these

310 activities are relatively low (0.016 and 0.057 dpm/ 100 L, respectively), they suggest that the
 311 waters downstream of the Leclaire Rise may be impacted by this topographic feature.
 312 However, sample UW-14 collected in surface waters lying above this rise does not show
 313 significant ^{223}Ra and ^{224}Ra activities and only low ^{228}Ra activity, which suggest that vertical
 314 mixing may not efficiently transport radium released by the shallow sediments towards
 315 surface waters above this topographic feature. Note that the influence of the Leclaire Rise on
 316 the chemical element concentrations downstream of the rise is also observed in Fe and other
 317 trace metal (REE, Mn, Al) concentrations, but only in waters lying in the 200-500 m depth
 318 interval (Bowie et al., 2014; van der Merwe et al., 2014; Grenier et al., in prep.).

319 4.2 Timescales of the offshore transport of surface waters

320 Once released into the water column, radium isotopes are subject to dilution, mixing
 321 and radioactive decay. The decay of short-lived radium isotopes in offshore waters provides
 322 information of how quickly chemical elements (including micronutrients) also released by the
 323 sediments are diluted and dispersed into the ocean (Moore, 2000). The presence of ^{224}Ra and
 324 ^{223}Ra in offshore waters thus indicates that the waters have recently been in interaction with
 325 the sediments. In contrast, when both ^{224}Ra and ^{223}Ra activities are below the detection limit,
 326 this suggests that the water bodies have not been in contact with the sediments over the past 2
 327 months (this is represented in light gray in Fig. 8). The water samples that display significant
 328 ^{223}Ra activity but no ^{224}Ra (represented in dark gray in Fig. 8) suggest that the interaction
 329 between the water body and the sediment occurred between 1 month (^{224}Ra activities < DL)
 330 and 2 months ago (significant ^{223}Ra activities). When both the ^{224}Ra and ^{223}Ra activities were
 331 significant, apparent ages could be calculated following (Moore, 2000) :

$$332 \quad t = \ln \frac{\left[\frac{^{224}\text{Ra}}{^{223}\text{Ra}} \right]_i}{\left[\frac{^{224}\text{Ra}}{^{223}\text{Ra}} \right]_{\text{obs}}} * \frac{1}{\lambda_{224} - \lambda_{223}} \quad (1)$$

333 where $(^{224}\text{Ra}/^{223}\text{Ra})_i$ is the initial ratio in source waters, $(^{224}\text{Ra}/^{223}\text{Ra})_{\text{obs}}$ is the ratio for a given
334 water sample, λ_{224} and λ_{223} are the decay constants of ^{224}Ra and ^{223}Ra , respectively. The
335 assumptions inherent to this equation can be found in Moore (2000) and are: (1) the ^{223}Ra and
336 ^{224}Ra activities are constant in the source region (i.e. a constant initial $^{224}\text{Ra}/^{223}\text{Ra}$ ratio is
337 assumed), (2) the $^{224}\text{Ra}/^{223}\text{Ra}$ ratio changes are only due to radioactive decay and (3) open
338 ocean waters contain no excess ^{223}Ra and ^{224}Ra .

339 In this study, we only reported the apparent ages deduced from the $^{224}\text{Ra}/^{223}\text{Ra}$ ratios
340 because we showed that both the ^{224}Ra and ^{223}Ra determined eastward of Kerguelen originate
341 from the shallow sediments of the Kerguelen Islands (see section 4.1). Apparent ages were
342 thus calculated using an initial $^{224}\text{Ra}/^{223}\text{Ra}$ ratio that was obtained by averaging the
343 ratios found in coastal water samples collected as close as possible to the radium source term
344 in the Baie du Morbihan (samples KER-1 and UW-36) and Baie des Baleiniers (samples
345 Baie-B1 and Baie-B2; Fig. 1). In contrast, we cannot exclude that ^{228}Ra has various origins
346 (Kerguelen Islands and/or Heard Island). The use of the $^{224}\text{Ra}/^{228}\text{Ra}$ or $^{223}\text{Ra}/^{228}\text{Ra}$ ratios to
347 derive apparent ages is thus compromised because it is not possible to determine a single
348 initial ratio in this case.

349 Several offshore samples display a young apparent age (4-8 days), suggesting a rapid
350 transport of radium between the shallow waters of the northern Kerguelen Plateau and
351 offshore. Station TNS1 located north of the PF is reached after 5 days. This observation
352 agrees with the circulation pattern in this area, with waters flowing eastward and that may
353 interact with the shallow northern Kerguelen Plateau (Park et al., 2014). This is also in
354 agreement with the drifters launched during the KEOPS 2 project that also highlighted such
355 advection along the PF (Fig. 7) (Zhou et al., 2014). Station UW-21 located ca. 50 km
356 offshore, station E1 and station UW-32 located ca. 200 km offshore also show relatively
357 young apparent ages (4, 5 and 6 days, respectively). Because all these stations are located

358 south of the PF, this suggests that the sediment-derived inputs may be rapidly transferred
359 towards offshore waters across the PF. Stations R-2 located south of the PF also displays a
360 young apparent age. At station Kerfix located close to station R-2, Jeandel et al. (1998)
361 reported westward currents associated with a recirculation pattern that may transport chemical
362 elements originating from the Kerguelen Plateau. The Ra signal may then be transported
363 eastward, as suggested by the significant ^{223}Ra activities also observed east of station R-2,
364 south of the PF (Fig. 4 and 8). Alternatively, the Leclaire Rise located west of R-2 may
365 impact the surface waters, thus leading to a young age for this water sample. Because the
366 ^{224}Ra and ^{223}Ra activities found at station A3-1 were attributed to the northward advection on
367 the southern Plateau, the apparent age at station A3-1 was calculated assuming that the initial
368 $^{224}\text{Ra}/^{223}\text{Ra}$ ratio off Heard Island is similar to that off Kerguelen Islands (Fig. 8). This
369 hypothesis may be correct since the geological contexts of the two islands are similar. The
370 apparent age thus calculated provides an estimate for the transit time of surface waters above
371 the southern Kerguelen Plateau between Heard Island and station A3. However, during the
372 second visit at station A3 (A3-2), the ^{224}Ra and ^{223}Ra activities were below the detection limit.
373 This may highlight the temporal variability in the circulation patterns in this area: the transit
374 time of surface waters between Heard Island and station A3 may thus vary with time, ranging
375 from one week to 1-2 months. On such timescales, the ^{228}Ra activities do not significantly
376 decay, which would explain why similar ^{228}Ra activities were found during the two visits at
377 A3. Finally, the spatial variability in the distribution of the apparent ages in offshore waters
378 suggests that the passage of chemical elements across the Polar Front is a sporadic process,
379 which may contribute to explain the mosaic structure of the phytoplankton bloom. Future
380 studies in the area could aim to track more precisely the sedimentary sources of radium (and
381 other chemical elements) and to quantify the radium fluxes out of the sediments using e.g. the
382 method developed by Cai et al. (2012).

383 4.3 Lagrangian particle analysis

384 To provide additional constraints on the origin of the Ra signal in offshore waters,
385 Lagrangian analyses derived from total surface currents were conducted at several stations
386 (Fig. 9). A two month backward analysis - to account for the life time of ^{223}Ra - was
387 performed starting from the sampling date for targets that were centered on the station
388 locations.

389 The Lagrangian analyses for the southern stations A3-1, A3-2, UW-35 and G-1 are
390 reported on Fig. 9. The backward trajectories provide a similar pattern and indicate a southern
391 origin for the surface waters found at these stations. This pattern agrees with the trajectories
392 of the two drifters released *in situ* at station A3 (Fig. 7). Waters that have interacted with the
393 shallow shelves of the southern Kerguelen Plateau (Heard Island) may thus reach the
394 investigated area. In particular, this northward advection may explain the significant Ra
395 activities determined at stations G-1 and A3-1. Note that the distance covered by the
396 backward trajectories over the 2 months is short, thus reflecting the relatively slow currents in
397 this area.

398 Lagrangian analyses were also performed for several northern stations: E-1, UW-31,
399 UW-32, TEW-7 and F-L. The trajectories are represented in shades of red on Fig. 9. Stations
400 F-L, TEW-7 and UW-31 are located relatively close to each other, east of the Kerguelen
401 Islands in the area of the southern branch of the cyclonic meander formed by the PF. Their
402 backward trajectories display a similar feature and all point to the same origin, which is the
403 northern Kerguelen Plateau. This suggests that chemical elements originating from the
404 Kerguelen Plateau may be transported offshore via the PF. The transit time given by the
405 Lagrangian analysis is approximately one month between the coast of the Kerguelen Islands
406 and the investigated stations. With a transit time of approximately one month, the ^{224}Ra

407 activities should have disappeared due to radioactive decay - or should be close to the
408 detection limit - while the ^{223}Ra activities should have significantly decayed. As a
409 comparison, the ^{224}Ra and ^{223}Ra activities are below the detection limit at stations F-L and
410 UW-31, whereas significant ^{223}Ra and ^{224}Ra activities were found at station TEW-7. Such
411 discrepancy between the investigated stations may highlight the spatial variability of the
412 circulation patterns in this area or that the Ra activities are close to the detection limits. Both
413 ^{224}Ra and ^{223}Ra activities are also significant at station E-1 located in the center of the
414 cyclonic meander formed by the PF. The Lagrangian analysis suggests that the surface waters
415 at station E-1 originate from the southwest. These waters flow northwards before reaching the
416 PF area and then follow the eastern shelf of the northern Kerguelen Plateau. When passing
417 close to the PF, these waters may receive significant Ra inputs (and potentially other
418 sediment-derived inputs) that could be transported via or across the front in this area. This Ra
419 signal may then be transferred to station E-1, as suggested by the backward trajectories. This
420 hypothesis is also supported by the study conducted by Zhou et al. (2014) who identified a
421 north-eastward drift of surface waters originating from the Kerguelen Plateau. Finally, the
422 backward trajectories at station UW-32 - that also displayed significant ^{223}Ra and ^{224}Ra -
423 highlight the spatial variability in that area: while several trajectories originate from the south,
424 several other trajectories follow the PF and the shelves of the northern Kerguelen Plateau,
425 where these waters could also potentially receive sediment-derived inputs.

426 4.4 Comparison of the apparent radium ages with an altimetry-based Lagrangian model

427 The timescale of the offshore transport of surface waters was also investigated using an
428 altimetry-based Lagrangian model (Fig. 10). The color bar indicates the time (number of
429 days) elapsed since the water body left the 2000 m-isobath. A color code similar to that of
430 Fig. 8 was used. A color palette from red to yellow highlights the rapid offshore transport of
431 the surface waters (surface waters < 6 days). The dark gray coding illustrates surface waters

432 that left the 2000 m-isobath less than 1 month ago. Finally, surface waters that left the 2000
433 m-isobath more than 1 month ago are represented in light gray. As a comparison, the radium
434 apparent ages are reported on the map using the same color code.

435 Young ages can be found close to the 2000 m-isobath, along the PF. Surface waters < 1
436 month follow the cyclonic meander formed by the PF, while waters older than 2 months are
437 found in the center of the meander. Note that the altimetry-derived Lagrangian analysis may
438 misplace structures with errors of ~10 km (e.g. d' Ovidio et al., 2010), which is comparable to
439 the width of the structures visible in the map. It may thus be difficult to compare
440 quantitatively the altimetry-derived ages with the ages determined *in situ*. Nevertheless, two
441 important considerations can be made: (i) the order of magnitude of the satellite-derived and
442 *in situ* ages are consistent in the region; (ii) considering a west-east transect from Kerguelen,
443 both estimations indicate a transition from young to old and then again young ages, which is
444 consistent with the existence of a retentive recirculation region centered at about 73 °W, 49
445 °S.

446 **5 Conclusion**

447 The observation of short-lived Ra isotopes (^{223}Ra and ^{224}Ra) in surface waters east of the
448 Kerguelen Islands, south of the PF clearly indicates that these waters have recently interacted
449 with shallow sediments. Neither the shelves of Heard Islands - located hundreds kilometers
450 south of the study area - nor the vertical mixing of deep waters that interacted with bottom
451 sediments can account for the short-lived radium enrichments found in surface waters. The
452 ^{223}Ra and ^{224}Ra activities south of the PF are thus best explained by waters that interacted
453 with the shelves of the Kerguelen Islands. This finding implies that chemical elements can be
454 transported across or via the PF. Among the potential mechanisms allowing surface waters to
455 be transported eastward across the PF, one can invoke either i) the wind stress (eastward

456 winds are especially strong in that region) or ii) eddies that form along the PF and that may
457 promote the transport of surface waters and associated chemical elements. The spatial
458 variability observed in the ^{223}Ra and ^{224}Ra distribution in surface waters south of the PF
459 suggests that the input of waters and associated chemical elements across the PF – potentially
460 driven by wind stress or eddies - act as sporadic pulses that may highly vary in both space and
461 time. This pathway may thus constitute a mechanism that contribute to fertilize the
462 phytoplankton bloom with iron and other micronutrients east of the Kerguelen Islands, south
463 of the PF. This finding shows that the PF may not act as a strong barrier for surface waters
464 and associated chemical elements, a finding that may also apply to other frontal systems of
465 the world's ocean.

466 **Author contribution**

467 P. van Beek and B. Lansard performed the sample collection on board the R/V Marion
468 Dufresne. The sample analysis was done on the ship by P. van Beek and B. Lansard and in the
469 laboratory by V. Sanial, and M. Souhaut. F. d'Ovidio developed the model code and E.
470 Kestenare performed the CTD analysis and the simulations for the Lagrangian analysis. M.
471 Zhou provided the drifter data. S. Blain is PI of the KEOPS-2 project and helped interpret the
472 data. V. Sanial interpreted the data and prepared the manuscript.

473 **Acknowledgements**

474 The authors would like to thank Bernard Quéguiner, chief scientist of the KEOPS-2 cruise.
475 We thank the captain and crew members of the R/V Marion Dufresne (IPEV-TAAF). We are
476 especially grateful to Pierre Sangiardi (IPEV) who designed the clean pump that allowed us to
477 collect surface water samples in this project. The altimeter current and color/temperature
478 products for the Kerguelen area were produced by Ssalto/Duacs and CLS with support from
479 CNES. This work was funded by the French Research program of INSU-CNRS LEFE-

480 CYBER (Les enveloppes fluides et l'environnement – Cycles biogéochimiques,
481 environnement et ressources), ANR (Agence Nationale de la Recherche, SIMI-6 program,
482 ANR-10-BLAN-0614), CNES (Centre National d'Etudes Spatiales) and IPEV (Institut
483 Polaire Paul-Emile Victor).

484 **Figure captions**

485 **Fig. 1.** Location of stations investigated for Ra analysis. Solid circles represent surface
486 seawater samples. Circles show the locations where vertical profiles were made. KP is the
487 abbreviation for Kerguelen Plateau.

488 **Fig. 2.** Satellite composite images of sea surface chlorophyll *a* (mg m^{-3}) at successive dates
489 between the beginning of the KEOPS-2 cruise (19/10/2011) and the end of the cruise
490 (23/11/2011). The location of the water samples collected for radium analysis within the
491 different time intervals is also reported (solid circles).

492 **Fig. 3.** Potential temperature-salinity diagrams at stations where radium analyses were
493 performed. F-L station is plotted in bold. TEW-3, G-1, E-1, E4-W and A3-2 stations are
494 plotted in gray. The main water masses are reported on the figure: Antarctic Surface Water
495 (AASW), SubAntarctic Surface Water (SASW), Winter Water (WW), Upper Circumpolar
496 Deep Water (UCDW), Lower Circumpolar Deep Water (LCDW) and Antarctic Bottom Water
497 (AABW).

498 **Fig. 4.** ^{224}Ra (A), ^{223}Ra (B) and ^{228}Ra (C) distributions in surface waters off the Kerguelen
499 Islands. Radium activities are expressed in dpm/ 100 L. White circles indicate samples with
500 Ra activity below the detection limit. A schematic view of the Polar Front (PF) is shown.

501 **Fig. 5.** Vertical profiles of ^{223}Ra , ^{224}Ra and ^{228}Ra activities (dpm/ 100 L) at the shallow
502 stations. The main water masses are indicated: Winter Water (WW), Upper Circumpolar Deep
503 Water (UCDW). The bottom depth is denoted by the horizontal lines.

504 **Fig. 6.** ^{223}Ra , ^{224}Ra and ^{228}Ra activities (dpm/ 100 L) at the deep stations. The major water
505 masses are indicated: Winter Water (WW), Upper Circumpolar Deep Water (UCDW), Lower

506 Circumpolar Deep Water (LCDW), Antarctic Bottom Water (AABW). The bottom depth is
507 denoted by the horizontal lines.

508 **Fig. 7.** Trajectories of the drifters launched eastward of the Kerguelen Islands during the
509 KEOPS-2 project. The trajectories of the two drifters released at station A3 are reported in
510 color. The equivalent transit time of the two drifters is reported in days along their trajectory.
511 The other drifter trajectories are represented in light grey.

512 **Fig. 8.** Apparent ages of surface waters determined using the $^{224}\text{Ra}/^{223}\text{Ra}$ ratios. The offshore
513 apparent ages were estimated using an initial $^{224}\text{Ra}/^{223}\text{Ra}$ ratio that was obtained by averaging
514 the ratios found at stations located on the northern Kerguelen Plateau (< 200 m water depth).
515 When both ^{224}Ra and ^{223}Ra were significant, apparent ages could be determined (colored
516 symbols). The samples displaying an apparent age between 1 and 2 months are shown in dark
517 gray ($^{224}\text{Ra} < \text{DL}$ but significant ^{223}Ra activities). Water samples displaying an apparent age >
518 2 months are shown in light grey ($^{224}\text{Ra} < \text{DL}$ and $^{223}\text{Ra} < \text{DL}$). A schematic view of the Polar
519 Front (PF) is represented.

520 **Fig. 9.** Lagrangian particle analysis derived from total surface currents (considering absolute
521 geostrophic plus Ekman currents). Solid circles represent the location of the stations. The
522 targets for Lagrangian analysis were centered on and around the station locations (to account
523 for spatial variability). The sampling date is indicated in brackets. Two month-backward
524 trajectories are shown. The first month is represented in bold.

525 **Fig. 10.** Ages of surface waters (in days) derived from an altimetry Lagrangian-based model.
526 *In-situ* ages derived from radium isotopes are represented by circles. The colorbar indicates
527 the time elapsed since the water body left the 2000-m isobath.

528

529

530 **References**

- 531 Annett, A. L., Henley, S. F., Van Beek, P., Souhaut, M., Ganeshram, R., Venables, H. J.,
532 Meredith, M. P. and Geibert, W.: Use of radium isotopes to estimate mixing rates and trace
533 sediment inputs to surface waters in northern Marguerite Bay, Antarctic Peninsula, Antarctic
534 Science, FirstView, 1–12, doi:10.1017/S0954102012000892, 2013.
- 535 Arrigo, K. R., Van Dijken, G. L. and Bushinsky, S.: Primary production in the Southern
536 Ocean, 1997–2006, Journal of Geophysical Research: Oceans, 113(C8),
537 doi:10.1029/2007JC004551, 2008.
- 538 De Baar, H. J. W., De Jong, J. T. M., Bakker, D. C. E., Löscher, B. M., Veth, C., Bathmann,
539 U. and Smetacek, V.: Importance of iron for plankton blooms and carbon dioxide drawdown
540 in the Southern Ocean, Nature, 373(6513), 412–415, doi:10.1038/373412a0, 1995.
- 541 Belkin, I. M. and Gordon, A. L.: Southern Ocean fronts from the Greenwich meridian to
542 Tasmania, Journal of Geophysical Research: Oceans, 101(C2), 3675–3696,
543 doi:10.1029/95JC02750, 1996.
- 544 Blain, S., Quéguiner, B., Armand, L., Belviso, S., Bombled, B., Bopp, L., Bowie, A., Brunet,
545 C., Brussaard, C., Carlotti, F., Christaki, U., Corbière, A., Durand, I., Ebersbach, F., Fuda, J.-
546 L., Garcia, N., Gerringa, L., Griffiths, B., Guigue, C., Guillerm, C., Jacquet, S., Jeandel, C.,
547 Laan, P., Lefèvre, D., Lo Monaco, C., Malits, A., Mosseri, J., Obernosterer, I., Park, Y.-H.,
548 Picheral, M., Pondaven, P., Remenyi, T., Sandroni, V., Sarthou, G., Savoye, N., Scouarnec,
549 L., Souhaut, M., Thuiller, D., Timmermans, K., Trull, T., Uitz, J., Van Beek, P., Veldhuis, M.,
550 Vincent, D., Viollier, E., Vong, L. and Wagener, T.: Effect of natural iron fertilization on
551 carbon sequestration in the Southern Ocean, Nature, 446(7139), 1070–1074,
552 doi:10.1038/nature05700, 2007.
- 553 Blain, S., Tréguer, P., Belviso, S., Bucciarelli, E., Denis, M., Desabre, S., Fiala, M., Martin
554 Jézéquel, V., Le Fèvre, J., Mayzaud, P., Marty, J.-C. and Razouls, S.: A biogeochemical study
555 of the island mass effect in the context of the iron hypothesis: Kerguelen Islands, Southern
556 Ocean, Deep Sea Research Part I: Oceanographic Research Papers, 48(1), 163–187,
557 doi:10.1016/S0967-0637(00)00047-9, 2001.
- 558 Bowie, A. R., Van der Merwe, P., Quéroué, F., Trull, T., Fourquez, M., Planchon, F., Sarthou,
559 G., Chever, F., Townsend, A. T., Obernosterer, I., Sallée, J.-B. and Blain, S.: Iron budgets for
560 three distinct biogeochemical sites around the Kerguelen archipelago (Southern Ocean)
561 during the natural fertilisation experiment KEOPS-2, Biogeosciences Discuss., 11(12),
562 17861–17923, doi:10.5194/bgd-11-17861-2014, 2014.
- 563 Cai, P., Shi, X., Moore, W. S. and Dai, M.: Measurement of ^{224}Ra : ^{228}Th disequilibrium in
564 coastal sediments using a delayed coincidence counter, Marine Chemistry, 138–139, 1–6,
565 doi:10.1016/j.marchem.2012.05.004, 2012.
- 566 Charette, M. A., Buesseler, K. O. and Andrews, J. E.: Utility of radium isotopes for evaluating
567 the input and transport of ground-water-driven nitrogen to a Cape Cod estuary, Limnology
568 and oceanography, 46(2), 465–470, 2001.
- 569 Charette, M. A., Gonnea, M. E., Morris, P. J., Statham, P., Fones, G., Planquette, H., Salter,
570 I. and Garabato, A. N.: Radium isotopes as tracers of iron sources fueling a Southern Ocean

- 571 phytoplankton bloom, *Deep Sea Research Part II: Topical Studies in Oceanography*, 54(18–
572 20), 1989–1998, doi:10.1016/j.dsr2.2007.06.003, 2007.
- 573 Charrassin, J.-B., Park, Y.-H., Le Maho, Y. and Bost, C.-A.: Fine resolution 3D temperature
574 fields off Kerguelen from instrumented penguins, *Deep Sea Research Part I: Oceanographic*
575 *Research Papers*, 51(12), 2091–2103, doi:10.1016/j.dsr.2004.07.019, 2004.
- 576 Chever, F., Sarthou, G., Bucciarelli, E., Blain, S. and Bowie, A. R.: An iron budget during the
577 natural iron fertilisation experiment KEOPS (Kerguelen Islands, Southern Ocean),
578 *Biogeosciences*, 7(2), 455–468, doi:10.5194/bg-7-455-2010, 2010.
- 579 Dibarboure, G., Pujol, M.-I., Briol, F., Traon, P. Y. L., Larnicol, G., Picot, N., Mertz, F. and
580 Ablain, M.: Jason-2 in DUACS: Updated System Description, First Tandem Results and
581 Impact on Processing and Products, *Marine Geodesy*, 34(3-4), 214–241,
582 doi:10.1080/01490419.2011.584826, 2011.
- 583 Dulaiova, H., Ardelan, M. V., Henderson, P. B. and Charette, M. A.: Shelf-derived iron inputs
584 drive biological productivity in the southern Drake Passage, *Global Biogeochemical Cycles*,
585 23(4), n/a–n/a, doi:10.1029/2008GB003406, 2009.
- 586 Emery, W. J. and Meincke, J.: Global water masses: summary and review, *Oceanologica acta*,
587 9(4), 383–391, 1986.
- 588 Garcia-Solsona, E., Garcia-Orellana, J., Masqué, P. and Dulaiova, H.: Uncertainties
589 associated with ²²³Ra and ²²⁴Ra measurements in water via a Delayed Coincidence Counter
590 (RaDeCC), *Marine Chemistry*, 109(3–4), 198–219, doi:10.1016/j.marchem.2007.11.006,
591 2008.
- 592 Grenier, M., Garcia-Solsona, E., Lemaitre, N., Bouvier, V., Nonnotte, P., Jeandel, C. :
593 Differentiating lithogenic supplies, water mass transport and biological processes on and off
594 the Kerguelen Plateau using the rare earth data, in prep.
- 595 Hanfland, C.: Radium-226 and Radium-228 in the Atlantic Sector of the Southern Ocean,
596 thesis, Alfred Wegener Institute, Bremerhaven Allemagne., 2002.
- 597 Jeandel, C., Ruiz-Pino, D., Gjata, E., Poisson, A., Brunet, C., Charriaud, E., dehaire, F.,
598 delille, D., Fiala, M., Fravallo, C., Carlos Miquel, J., Park, Y., Pondaven, P., Queguiner, B.,
599 Razouls, S., Shauer, B. and Treguer, P.: KERFIX, a time-series station in the Southern Ocean:
600 a presentation, *Journal of Marine Systems*, 17(1), 555–569, doi:10.1016/S0924-
601 7963(98)00064-5, 1998.
- 602 Kaufman, A., Trier, R. M., Broecker, W. S. and Feely, H. W.: Distribution of ²²⁸Ra in the
603 world ocean, *Journal of Geophysical Research*, 78(36), 8827–8848,
604 doi:10.1029/JC078i036p08827, 1973.
- 605 Korb, R. E., Whitehouse, M. J. and Ward, P.: SeaWiFS in the southern ocean: spatial and
606 temporal variability in phytoplankton biomass around South Georgia, *Deep Sea Research Part*
607 *II: Topical Studies in Oceanography*, 51(1–3), 99–116, doi:10.1016/j.dsr2.2003.04.002, 2004.
- 608 Martin, J. H., Fitzwater, S. E. and Gordon, R. M.: Iron deficiency limits phytoplankton
609 growth in Antarctic waters, *Global Biogeochemical Cycles*, 4(1), 5–12,
610 doi:10.1029/GB004i001p00005, 1990.

611 van der Merwe, P., Bowie, A. R., Qu  rou  , F., Armand, L., Blain, S., Chever, F., Davies, D.,
612 Dehairs, F., Planchon, F., Sarthou, G., Townsend, A. T. and Trull, T.: Sourcing the iron in the
613 naturally-fertilised bloom around the Kerguelen Plateau: particulate trace metal dynamics,
614 *Biogeosciences Discuss.*, 11(9), 13389–13432, doi:10.5194/bgd-11-13389-2014, 2014.

615 Mongin, M. M., Abraham, E. R. and Trull, T. W.: Winter advection of iron can explain the
616 summer phytoplankton bloom that extends 1000 km downstream of the Kerguelen Plateau in
617 the Southern Ocean, *Journal of Marine Research*, 67(2), 225–237,
618 doi:10.1357/002224009789051218, 2009.

619 Moore, J. K. and Abbott, M. R.: Surface chlorophyll concentrations in relation to the
620 Antarctic Polar Front: seasonal and spatial patterns from satellite observations, *Journal of*
621 *Marine Systems*, 37(1–3), 69–86, doi:10.1016/S0924-7963(02)00196-3, 2002.

622 Moore, W. S.: Ages of continental shelf waters determined from ²²³Ra and ²²⁴Ra, *Journal of*
623 *Geophysical Research*, 105(C9), 22117, doi:10.1029/1999JC000289, 2000.

624 Moore, W. S.: Fifteen years experience in measuring ²²⁴Ra and ²²³Ra by delayed-
625 coincidence counting, *Marine Chemistry*, 109(3-4), 188–197,
626 doi:10.1016/j.marchem.2007.06.015, 2008.

627 Moore, W. S. and Arnold, R.: Measurement of ²²³Ra and ²²⁴Ra in coastal waters using a
628 delayed coincidence counter, *Journal of Geophysical Research: Oceans*, 101(C1), 1321–1329,
629 doi:10.1029/95JC03139, 1996.

630 Orsi, A. H., Whitworth III, T. and Nowlin Jr., W. D.: On the meridional extent and fronts of
631 the Antarctic Circumpolar Current, *Deep Sea Research Part I: Oceanographic Research*
632 *Papers*, 42(5), 641–673, doi:10.1016/0967-0637(95)00021-W, 1995.

633 d’ Ovidio, F., De Monte, S., Alvain, S., Dandonneau, Y. and Levy, M.: Fluid dynamical
634 niches of phytoplankton types, *Proc Natl Acad Sci U S A*, 107(43), 18366–18370,
635 doi:10.1073/pnas.1004620107, 2010.

636 Park, Charriaud E. and Fieux M.: Thermohaline structure of the Antarctic Surface
637 Water/Winter Water in the Indian sector of the Southern Ocean, *Journal of Marine Systems*,
638 17(1), 5–23, doi:10.1016/S0924-7963(98)00026-8, 1998a.

639 Park, Y.-H., Charriaud, E., Pino, D. R. and Jeandel, C.: Seasonal and interannual variability of
640 the mixed layer properties and steric height at station KERFIX, southwest of Kerguelen,
641 *Journal of Marine Systems*, 17(1-4), 571–586, doi:10.1016/S0924-7963(98)00065-7, 1998b.

642 Park, Y.-H., Durand, I., Kestenare, E., Rougier, G., Zhou, M., D’ Ovidio, F., Cott  , C. and
643 Lee, J.-H.: Polar Front around the Kerguelen Islands: An up-to-date determination and
644 associated circulation of surface/subsurface waters, *J. Geophys. Res. Oceans*,
645 doi:10.1002/2014JC010061, 2014.

646 Park, Y.-H., Fuda, J.-L., Durand, I. and Naveira Garabato, A. C.: Internal tides and vertical
647 mixing over the Kerguelen Plateau, *Deep Sea Research Part II: Topical Studies in*
648 *Oceanography*, 55(5-7), 582–593, doi:10.1016/j.dsr2.2007.12.027, 2008a.

- 649 Park, Y.-H. and Gamberoni, L.: Cross-frontal exchange of Antarctic Intermediate Water and
650 Antarctic Bottom Water in the Crozet Basin, *Deep Sea Research Part II: Topical Studies in*
651 *Oceanography*, 44(5), 963–986, doi:10.1016/S0967-0645(97)00004-0, 1997.
- 652 Park, Y.-H. and Gambéroni, L.: Large-scale circulation and its variability in the south Indian
653 Ocean from TOPEX/POSEIDON altimetry, *Journal of Geophysical Research: Oceans*,
654 100(C12), 24911–24929, doi:10.1029/95JC01962, 1995.
- 655 Park, Y.-H., Gamberoni, L. and Charriaud, E.: Frontal structure, water masses, and circulation
656 in the Crozet Basin, *Journal of Geophysical Research*, 98(C7), 12361,
657 doi:10.1029/93JC00938, 1993.
- 658 Park, Y.-H., Roquet, F., Durand, I. and Fuda, J.-L.: Large-scale circulation over and around
659 the Northern Kerguelen Plateau, *Deep Sea Research Part II: Topical Studies in*
660 *Oceanography*, 55(5-7), 566–581, doi:10.1016/j.dsr2.2007.12.030, 2008b.
- 661 Park, Y.-H., Vivier, F., Roquet, F. and Kestenare, E.: Direct observations of the ACC
662 transport across the Kerguelen Plateau, *Geophysical Research Letters*, 36(18),
663 doi:10.1029/2009GL039617, 2009.
- 664 Pollard, R. ., Lucas, M. . and Read, J. .: Physical controls on biogeochemical zonation in the
665 Southern Ocean, *Deep Sea Research Part II: Topical Studies in Oceanography*, 49(16), 3289–
666 3305, doi:10.1016/S0967-0645(02)00084-X, 2002.
- 667 Pollard, R., Sanders, R., Lucas, M. and Statham, P.: The Crozet Natural Iron Bloom and
668 Export Experiment (CROZEX), *Deep Sea Research Part II: Topical Studies in Oceanography*,
669 54(18–20), 1905–1914, doi:10.1016/j.dsr2.2007.07.023, 2007.
- 670 Quéroué, F., Sarthou, G., Planquette, H.F., Bucciarelli, F., Chever, F., van der Merwe, P.,
671 Lannuzel, D., Townsend, A.T., Cheize, M., Blain, S., d'Ovidio, F. and Bowie, A.: High
672 variability of dissolved iron concentrations in the vicinity of Kerguelen Island (Southern
673 Ocean) submitted to *Biogeosciences*.
- 674 Sanial, V., Van Beek, P., Lansard, B., D' Ovidio, F., Kestenare, E., Souhaut, M., Zhou, M.
675 and Blain, S.: Study of the phytoplankton plume dynamics off the Crozet Islands (Southern
676 Ocean): A geochemical-physical coupled approach, *J. Geophys. Res. Oceans*, 119, 2227–
677 2237, doi:10.1002/2013JC009305, 2014.
- 678 Tagliabue, A., Sallée, J.-B., Bowie, A. R., Lévy, M., Swart, S. and Boyd, P. W.: Surface-
679 water iron supplies in the Southern Ocean sustained by deep winter mixing, *Nature Geosci*,
680 7(4), 314–320, doi:10.1038/ngeo2101, 2014.
- 681 van Beek, P., Bourquin, M., Reyss, J.-L., Souhaut, M., Charette, M. A. and Jeandel, C.:
682 Radium isotopes to investigate the water mass pathways on the Kerguelen Plateau (Southern
683 Ocean), *Deep Sea Research Part II: Topical Studies in Oceanography*, 55(5-7), 622–637,
684 doi:10.1016/j.dsr2.2007.12.025, 2008.
- 685 van Beek, P., Souhaut, M., Lansard, B., Bourquin, M., Reyss, J.-L., Von Ballmoos, P. and
686 Jean, P.: LAFARA: a new underground laboratory in the French Pyrenees for ultra low-level
687 gamma-ray spectrometry, *J. Environ. Radioact.*, 116, 152–158,
688 doi:10.1016/j.jenvrad.2012.10.002, 2013.

- 689 van Beek, P., Souhaut, M. and Reyss, J.-L.: Measuring the radium quartet (^{228}Ra , ^{226}Ra ,
690 ^{224}Ra , ^{223}Ra) in seawater samples using gamma spectrometry, *Journal of Environmental*
691 *Radioactivity*, 101(7), 521–529, doi:10.1016/j.jenvrad.2009.12.002, 2010.
- 692 Weis, D. and Frey, F. A.: Submarine Basalts of the Northern Kerguelen Plateau: Interaction
693 Between the Kerguelen Plume and the Southeast Indian Ridge Revealed at ODP Site 1140, *J.*
694 *Petrology*, 43(7), 1287–1309, doi:10.1093/petrology/43.7.1287, 2002.
- 695 Zhang, Y., Lacan, F. and Jeandel, C.: Dissolved rare earth elements tracing lithogenic inputs
696 over the Kerguelen Plateau (Southern Ocean), *Deep Sea Research Part II: Topical Studies in*
697 *Oceanography*, 55(5–7), 638–652, doi:10.1016/j.dsr2.2007.12.029, 2008.
- 698 Zhou, M., Zhu, Y., D’Ovidio, F., Park, Y.-H., Durand, I., Kestenare, E., Sanial, V., Van-
699 Beek, P., Queguiner, B., Carlotti, F. and Blain, S.: Surface currents and upwelling in
700 Kerguelen Plateau regions, *Biogeosciences Discuss.*, 11(5), 6845–6876, doi:10.5194/bgd-11-
701 6845-2014, 2014.

702

703

704 **Table 1:** Dissolved ^{223}Ra , ^{224}Ra and ^{228}Ra activities determined in surface samples collected off the
705 Kerguelen Islands. The ^{223}Ra and ^{224}Ra activities are excess radium activities (see Methods for details).
706 Activities are expressed in disintegration per minute per 100 L (dpm/ 100 L). <DL = Below the
707 Detection Limit.

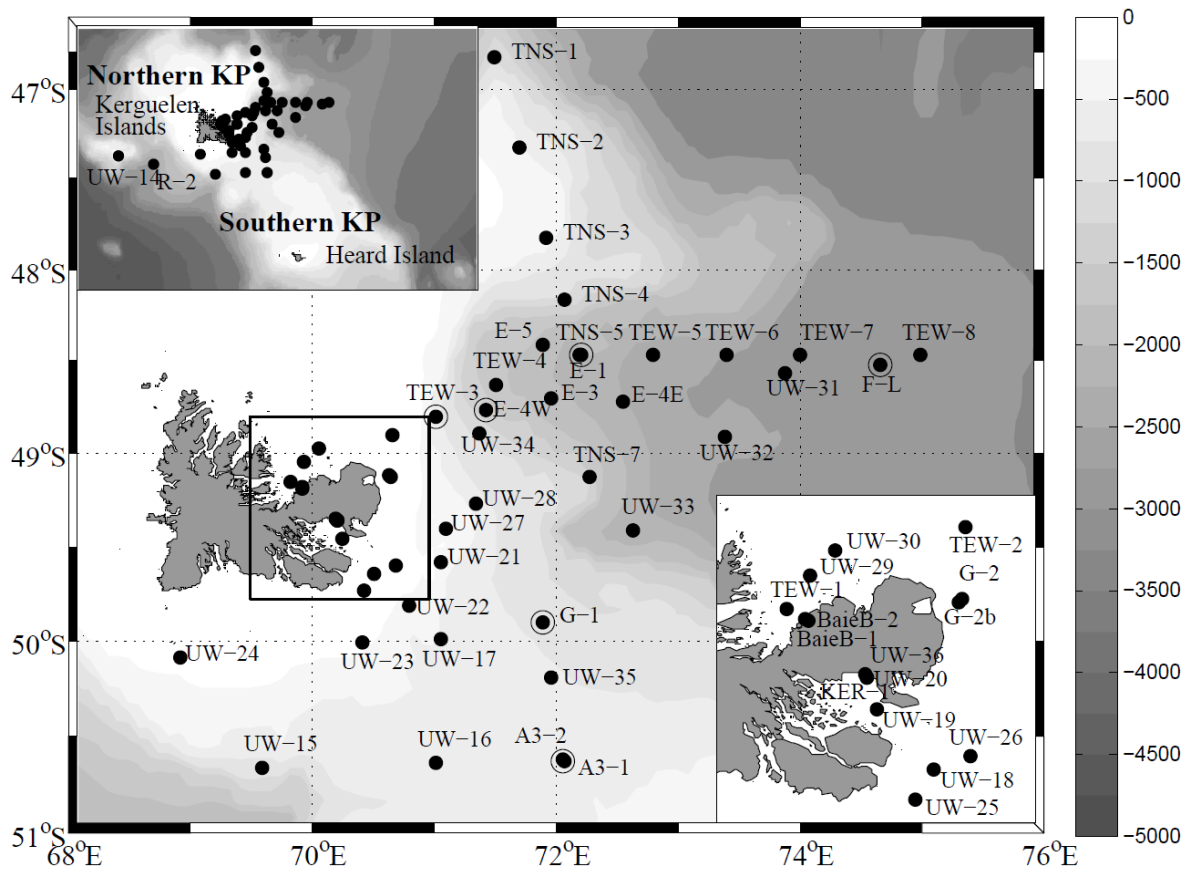
708 **Table 2:** Dissolved ^{223}Ra , ^{224}Ra and ^{228}Ra activities determined in seawater samples collected in the
709 water column using Niskin bottles. The ^{223}Ra and ^{224}Ra activities are excess radium activities (See
710 Methods for details). Activities are expressed in disintegration per minute per 100 L (dpm/ 100 L). The
711 number of counts detected using the RaDeCC is also reported in the Table (cnts). <DL = Below the
712 Detection Limit.

Station	Sampling Date	Volume (L)	Depth (m)	Bottom Depth (m)	²²³ Ra		²²⁴ Ra		²²⁸ Ra		²²³ Ra/ ²²⁸ Ra		²²⁴ Ra/ ²²⁸ Ra		²²⁴ Ra/ ²²³ Ra		
					(dpm/ 100 L)		(dpm/ 100 L)		(dpm/ 100 L)								
UW-14	17/10/2011 12:10	900	7	342	< LD		< LD		0.06 ± 0.019								
UW-15	18/10/2011 05:43	900	7	712	0.008	±	0.006	< LD		0.03 ± 0.010		0.24 ± 0.19					
UW-16	18/10/2011 09:50	900	7	560	0.007	±	0.007	< LD		0.05 ± 0.013		0.13 ± 0.13					
UW-17	19/10/2011 22:03	500	7	676	< LD		< LD		0.17 ± 0.035								
UW-18	19/10/2011 01:30	250	7	104	0.062	±	0.018	0.213 ± 0.062		0.49 ± 0.079		0.13 ± 0.04		0.44 ± 0.15		3.45 ± 1.41	
UW-19	19/10/2011 01:30	250	7	160	0.047	±	0.016	0.143 ± 0.052		0.47 ± 0.139		0.10 ± 0.05		0.31 ± 0.14		3.03 ± 1.51	
UW-20	19/10/2011 04:15	250	7		0.090	±	0.020	0.808 ± 0.079		1.21 ± 0.082		0.07 ± 0.02		0.67 ± 0.08		8.98 ± 2.15	
UW-21	24/10/2011 10:46	700	7	597	0.011	±	0.005	0.036 ± 0.024		0.11 ± 0.026		0.10 ± 0.05		0.33 ± 0.24		3.38 ± 2.69	
UW-22	24/10/2011 12:10	450	7	253	0.023	±	0.007	< LD		0.20 ± 0.039		0.11 ± 0.04					
UW-23	24/10/2011 14:05	450	7	233	0.008	±	0.006	0.116 ± 0.025		0.04 ± 0.013		0.19 ± 0.16		2.92 ± 1.16		15.17 ± 11.93	
UW-24	24/10/2011 23:37	450	7	171	< LD		< LD		0.11 ± 0.020								
UW-25	28/10/2011 03:40	700	7	116	0.060	±	0.011	0.218 ± 0.055		0.08 ± 0.017		0.72 ± 0.19		2.62 ± 0.84		3.64 ± 1.11	
UW-26	28/10/2011 04:35	700	7	130	0.043	±	0.010	0.065 ± 0.033		0.19 ± 0.023		0.23 ± 0.06		0.34 ± 0.18		1.50 ± 0.84	
UW-27	28/10/2011 06:00	500	7	393	0.019	±	0.007	< LD		0.06 ± 0.016		0.31 ± 0.14					
UW-28	28/10/2011 06:55	700	7	650	0.020	±	0.008	< LD		0.07 ± 0.015		0.29 ± 0.13					
UW-29	31/10/2011 07:44	450	7	100	0.031	±	0.011	0.118 ± 0.045		0.53 ± 0.038		0.06 ± 0.02		0.22 ± 0.09		3.81 ± 2.02	
UW-30	31/10/2011 08:17	450	7	100	0.083	±	0.014	0.201 ± 0.039		0.58 ± 0.039		0.14 ± 0.03		0.35 ± 0.07		2.44 ± 0.62	
UW-31	05/11/2011 12:20	700	7		< LD		< LD		0.17 ± 0.027								
UW-32	08/11/2011 08:50	700	7	4561	0.013	±	0.008	0.035 ± 0.046		0.24 ± 0.040		0.05 ± 0.04		0.15 ± 0.19		2.82 ± 4.10	
UW-33	08/11/2011 13:17	450	7	1664	< LD		< LD		0.09 ± 0.030								
UW-34	09/11/2011 01:50	500	7	1118	0.017	±	0.011	0.124 ± 0.078		0.10 ± 0.020		0.16 ± 0.12		1.23 ± 0.80		7.45 ± 6.84	
UW-35	17/11/2011 16:41	700	7	554	< LD		< LD		0.16 ± 0.026								
UW-36	21/11/2011 05:25	500	7	21	0.098	±	0.016	0.411 ± 0.098		1.07 ± 0.054		0.09 ± 0.02		0.38 ± 0.09		4.18 ± 1.22	
UW-37	22/11/2011 08:35	900	7	3720	< LD		< LD		0.13 ± 0.016								
TNS-1	23/10/2011 11:55	500	7	2280	0.015	±	0.005	0.046 ± 0.033		0.07 ± 0.022		0.21 ± 0.10		0.65 ± 0.50		3.11 ± 2.46	
TNS-2	23/10/2011 07:00	700	7	520	0.023	±	0.006	< LD		0.31 ± 0.064		0.07 ± 0.02					
TNS-3	23/10/2011 03:23	700	7	540	0.006	±	0.004	< LD		0.15 ± 0.050		0.04 ± 0.03					
TNS-4	22/10/2011 19:30	700	7	1800	0.015	±	0.005	< LD		0.08 ± 0.017		0.20 ± 0.08					
TNS-5	22/10/2011 11:55	700	7	2060	0.021	±	0.005	0.070 ± 0.030		0.17 ± 0.050		0.13 ± 0.05		0.42 ± 0.22		3.26 ± 1.62	
TNS-7	21/10/2011 20:25	700	7	1864	< LD		< LD		0.03 ± 0.012								
TEW-1	31/10/2011 05:56	700	7	92	0.014	±	0.011	0.131 ± 0.045		0.84 ± 0.051		0.02 ± 0.01		0.16 ± 0.05		9.31 ± 7.86	
TEW-2	31/10/2011 10:40	450	7	85	0.039	±	0.011	0.153 ± 0.045		0.28 ± 0.027		0.14 ± 0.04		0.55 ± 0.17		3.89 ± 1.56	
TEW-3	31/10/2011 17:35	500	7	557	0.008	±	0.007	< LD		0.10 ± 0.018		0.08 ± 0.07					
TEW-4	01/11/2011 03:45	500	7	1596	< LD		< LD		0.08 ± 0.025								
TEW-5	01/11/2011 16:05	450	7	2290	< LD		0.128 ± 0.044		0.18 ± 0.033				0.71 ± 0.28				
TEW-6	02/11/2011 00:05	450	7	2400	0.011	±	0.006	< LD		0.08 ± 0.019		0.13 ± 0.08					
TEW-7	02/11/2011 05:15	700	7	2510	0.020	±	0.009	0.147 ± 0.062		0.16 ± 0.019		0.13 ± 0.06		0.93 ± 0.40		7.37 ± 4.51	
TEW-8	02/11/2011 17:40	900	7	2800	< LD		< LD		0.17 ± 0.024								
E-1	29/10/2011 10:55	900	7	2065	0.021	±	0.005	0.070 ± 0.022		0.10 ± 0.022		0.23 ± 0.08		0.73 ± 0.28		3.26 ± 1.29	
E-3	03/11/2011 16:15	900	7	1915	0.009	±	0.005	< LD		0.03 ± 0.016		0.33 ± 0.25					
E-4W	12/11/2011 06:15	900	7	1385	0.010	±	0.007	< LD		0.14 ± 0.034							
E-4E	12/11/2011 08:37	500	7	2210	< LD		< LD		0.12 ± 0.021								
E-5	18/11/2011 00:25	900	7	1920	< LD		< LD		0.11 ± 0.008								
A3-1	19/10/2011 19:15	900	7	528	0.015	±	0.003	0.034 ± 0.024		0.12 ± 0.041		0.12 ± 0.05		0.28 ± 0.21		2.26 ± 1.62	
A3-2	19/10/2011 19:15	900	7	531	< LD		< LD		0.12 ± 0.024								
G-1	09/11/2011 05:20	900	7	592	0.023	±	0.007	< LD		0.05 ± 0.020		0.46 ± 0.23					
G-2	09/11/2011 14:10	500	7	67	0.089	±	0.015	0.412 ± 0.052		0.36 ± 0.046		0.25 ± 0.05		1.15 ± 0.21		4.64 ± 0.98	
G-2b	21/11/2011 11:00	500	7	67	0.130	±	0.017	0.568 ± 0.067		0.75 ± 0.066		0.17 ± 0.03		0.75 ± 0.11		4.36 ± 0.77	
F-L	06/11/2011 13:33	900	7	2670	< LD		< LD		0.17 ± 0.021								
R-2	26/10/2011 02:40	900	7	2531	0.016	±	0.009	0.057 ± 0.028		0.11 ± 0.016		0.15 ± 0.09		0.53 ± 0.27		3.49 ± 2.51	
KER-1	19/10/2011 04:45	87.8	1	3	0.302	±	0.048	2.053 ± 0.125		1.62 ± 0.160		0.19 ± 0.03		1.27 ± 0.15		6.80 ± 1.16	
BaieB-1	31/10/2011 05:00	99.3	1	3	0.219	±	0.032	2.332 ± 0.118		0.88 ± 0.089		0.25 ± 0.04		2.65 ± 0.30		10.67 ± 1.67	
BaieB-2	40847.20833	65.2	1	3	0.012	±	0.008	0.256 ± 0.024		2.57 ± 0.183		0.005 ± 0.003		0.10 ± 0.01		20.64 ± 13.83	

Station and Depth (m)	Volume (L)	Bottom Depth (m)	²²³ Ra (dpm/ 100 L)	²²³ Ra cnts	²²⁴ Ra (dpm/ 100 L)	²²⁴ Ra cnts	²²⁸ Ra (dpm/ 100 L)	²²⁸ Ra cnts
E-1								
182	256	2065	< LD		0.041 ± 0.031	134	0.03 ± 0.01	44
508	263	2065	0.019 ± 0.012	38	< LD		< LD	
1013	262	2065	0.010 ± 0.009	24	< LD		0.07 ± 0.015	78
1623	256	2065	0.058 ± 0.013	74	< LD		0.22 ± 0.034	134
2069	274	2065	0.170 ± 0.024	180	0.045 ± 0.037	344	0.23 ± 0.033	141
TEW-3								
101	259	557	< LD		< LD		0.29 ± 0.068	125
303	257	557	0.039 ± 0.013	37	0.065 ± 0.052	129	0.28 ± 0.037	154
557	252	557	0.014 ± 0.015	33	0.077 ± 0.056	213	0.37 ± 0.098	68
F-L								
101	257	2670	0.008 ± 0.007	17	< LD		0.20 ± 0.130	49
183	260	2670	< LD		0.086 ± 0.022	246	0.19 ± 0.054	35
405	258	2670	0.016 ± 0.009	24	< LD		0.06 ± 0.030	22
907	258	2670	0.039 ± 0.012	46	0.103 ± 0.060	107	0.12 ± 0.044	28
1825	122	2670	0.064 ± 0.017	32	0.128 ± 0.077	239	0.54 ± 0.130	49
2723	124	2670	0.142 ± 0.049	123	0.265 ± 0.154	346	0.93 ± 0.097	290
G-1								
10	269	592	< LD		< LD		0.38 ± 0.042	187
53	251	592	0.020 ± 0.009	30	0.051 ± 0.049	107	0.31 ± 0.039	157
130	255	592	< LD		< LD		0.26 ± 0.066	43
303	260	592	< LD		< LD		0.38 ± 0.081	56
455	234	592	< LD		< LD		0.29 ± 0.074	44
576	223	592	0.088 ± 0.021	84	0.075 ± 0.058	75	0.36 ± 0.077	48
E-4W								
94	261	1385	0.020 ± 0.014	31	< LD		0.34 ± 0.079	50
192	260	1385	< LD		< LD		0.30 ± 0.041	135
608	253	1385	< LD		< LD		0.29 ± 0.043	151
1013	123	1385	< LD		0.133 ± 0.046	93	0.43 ± 0.116	36
1383	123	1385	0.057 ± 0.021	25	0.071 ± 0.046	145	0.90 ± 0.164	59
A3-2								
101	258	531	< LD		< LD		0.10 ± 0.042	25
152	246	531	< LD		< LD		0.16 ± 0.029	115
233	258	531	< LD		< LD		0.18 ± 0.060	33
303	124	531	< LD		< LD		0.49 ± 0.125	39
404	110	531	< LD		< LD		0.68 ± 0.156	44
518	246	531	0.081 ± 0.019	58	< LD		0.70 ± 0.102	82
TEW-1								
82	258.5	92	0.053 ± 0.015	49	0.125 ± 0.059	334	0.88 ± 0.083	197
TEW-8								
20	269	2800	0.011 ± 0.009	22	< LD	335	0.14 ± 0.032	69
G-2								
50	229.6	67	0.094 ± 0.022	65	0.737 ± 0.097	389	0.79 ± 0.083	167

714 Fig. 1.

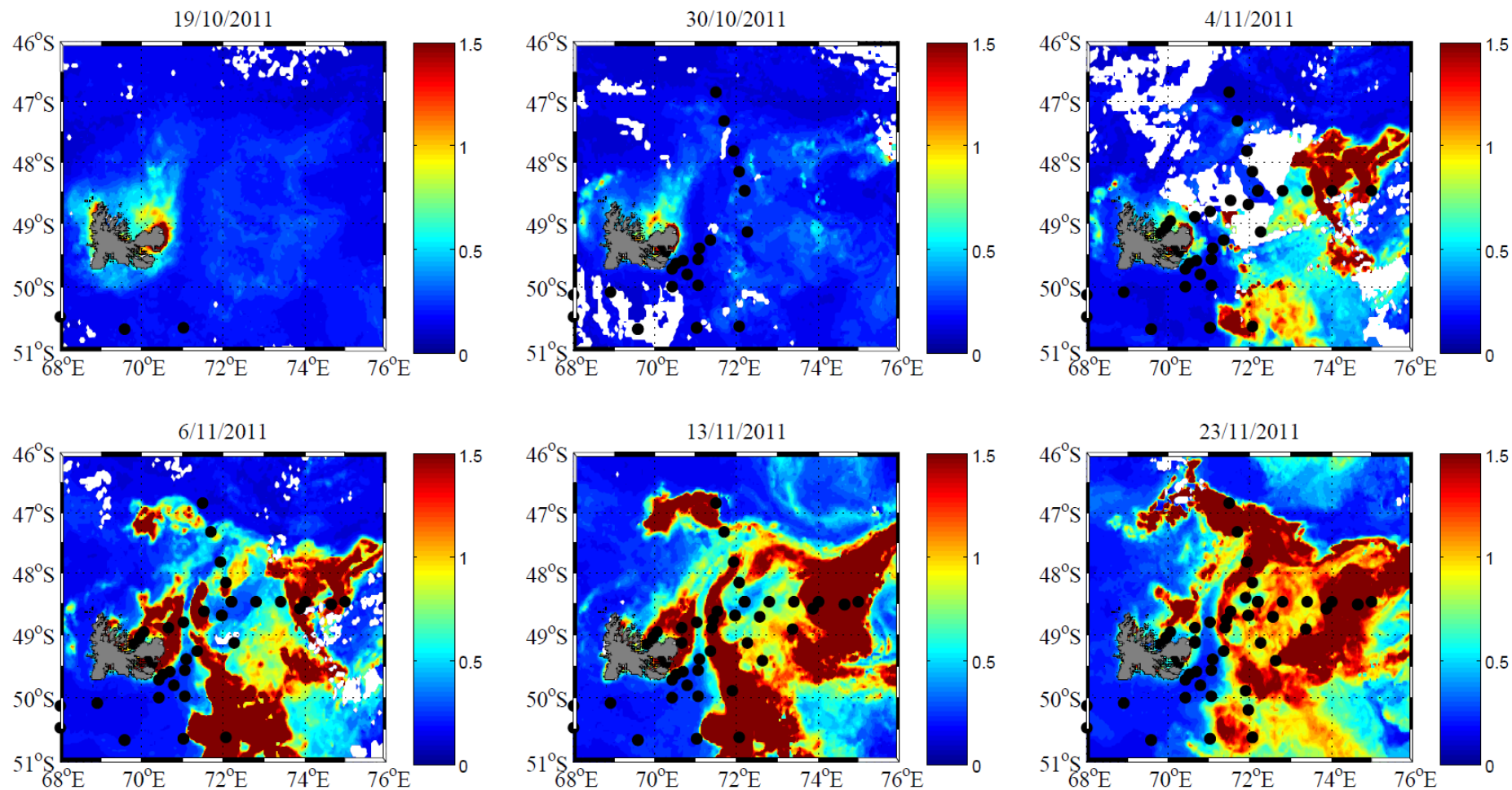
715



716

717

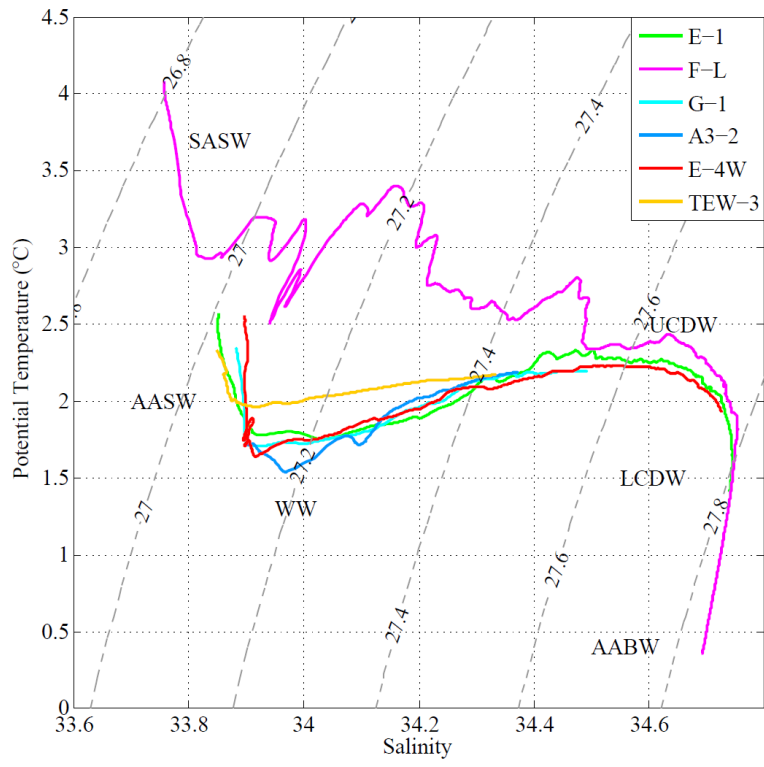
718 Fig. 2.



719

720

721 Fig. 3.



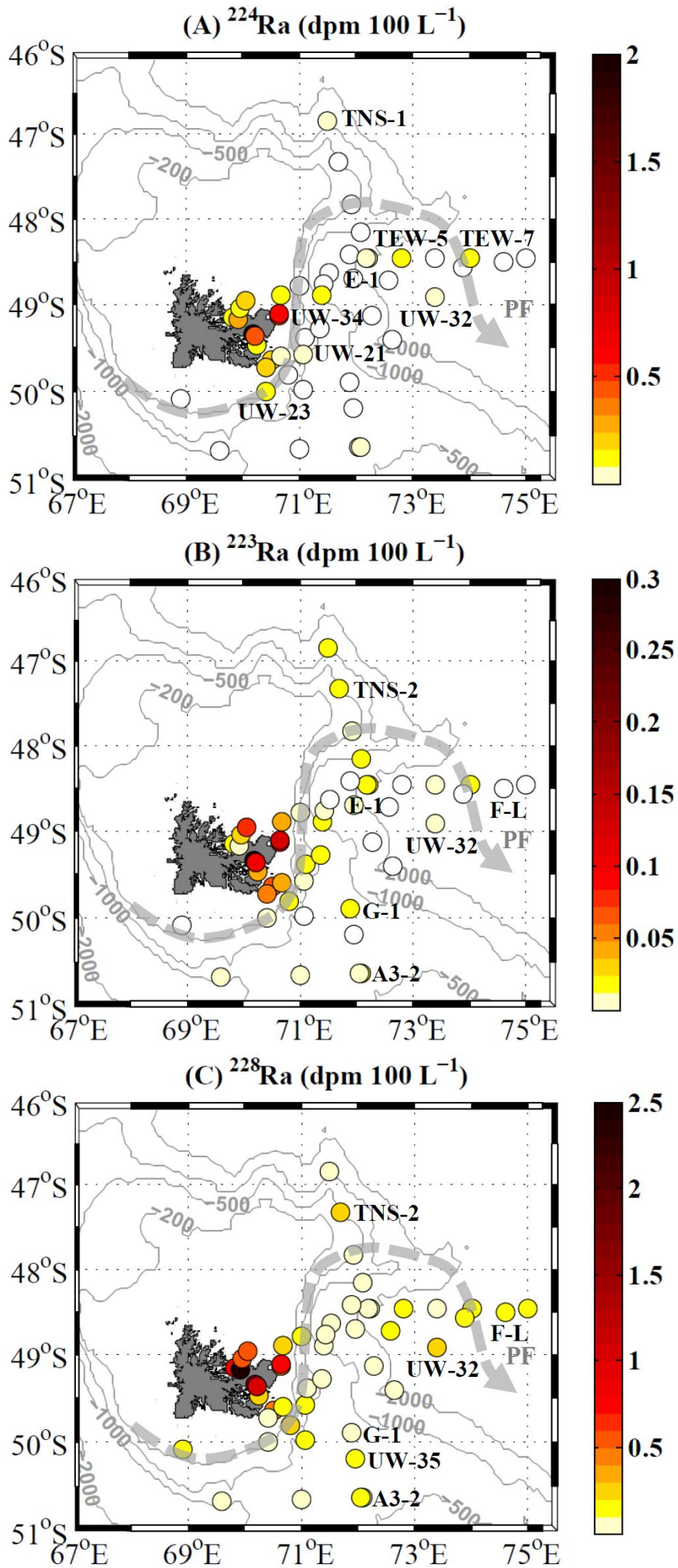
722

723

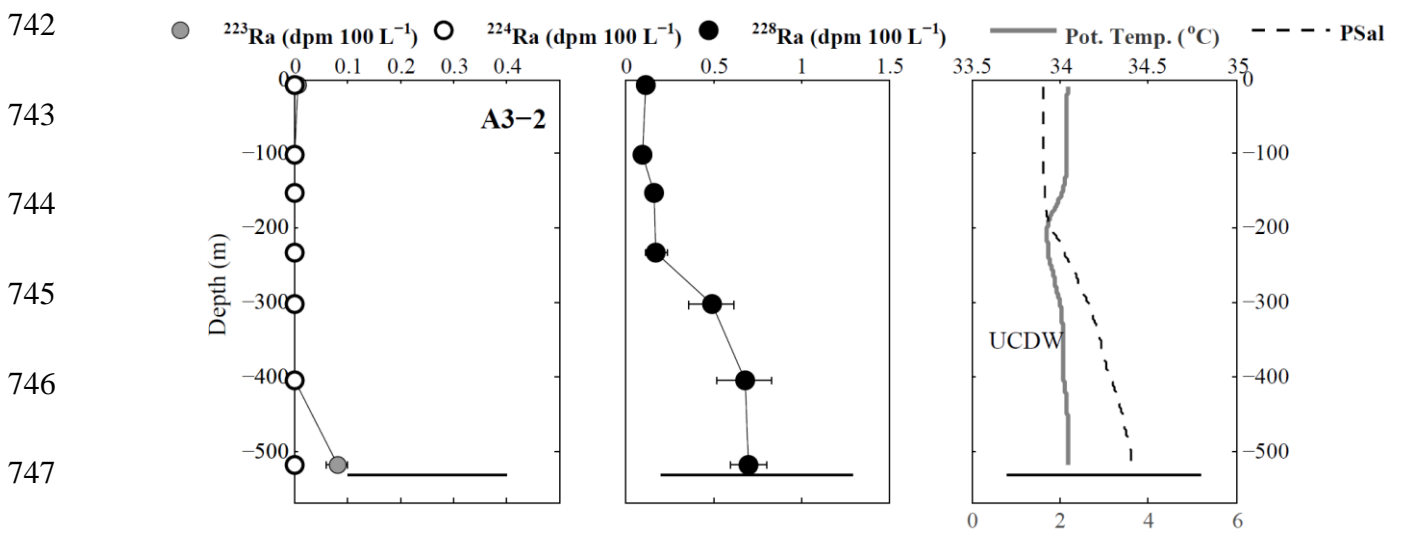
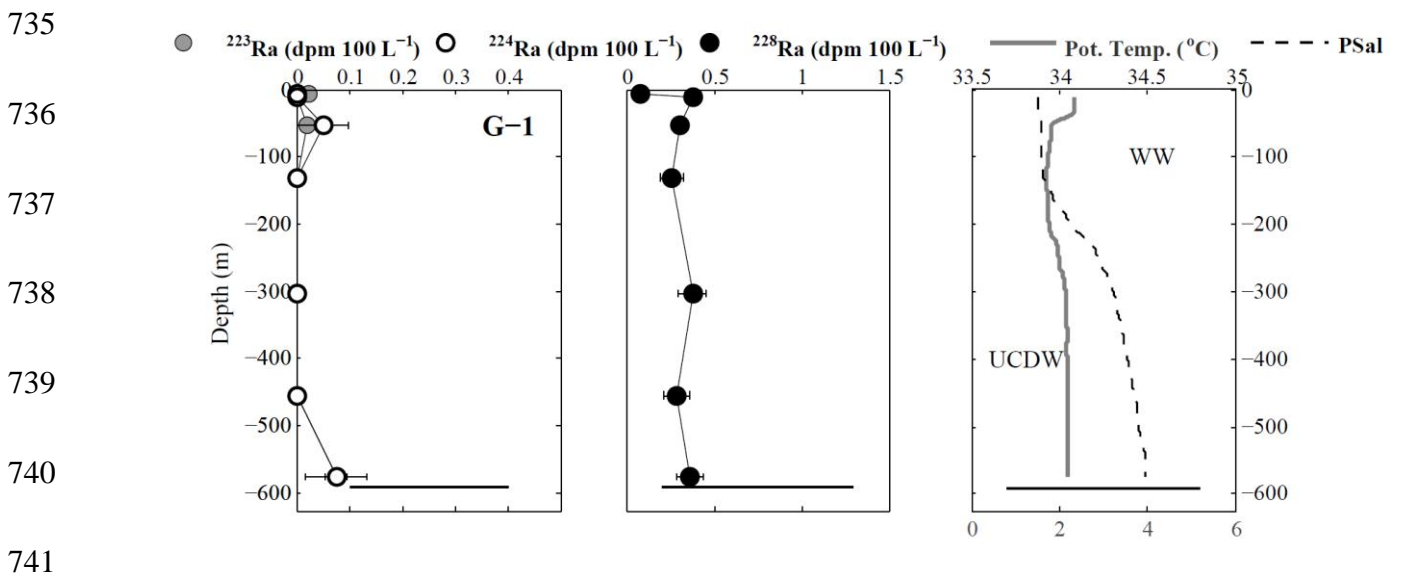
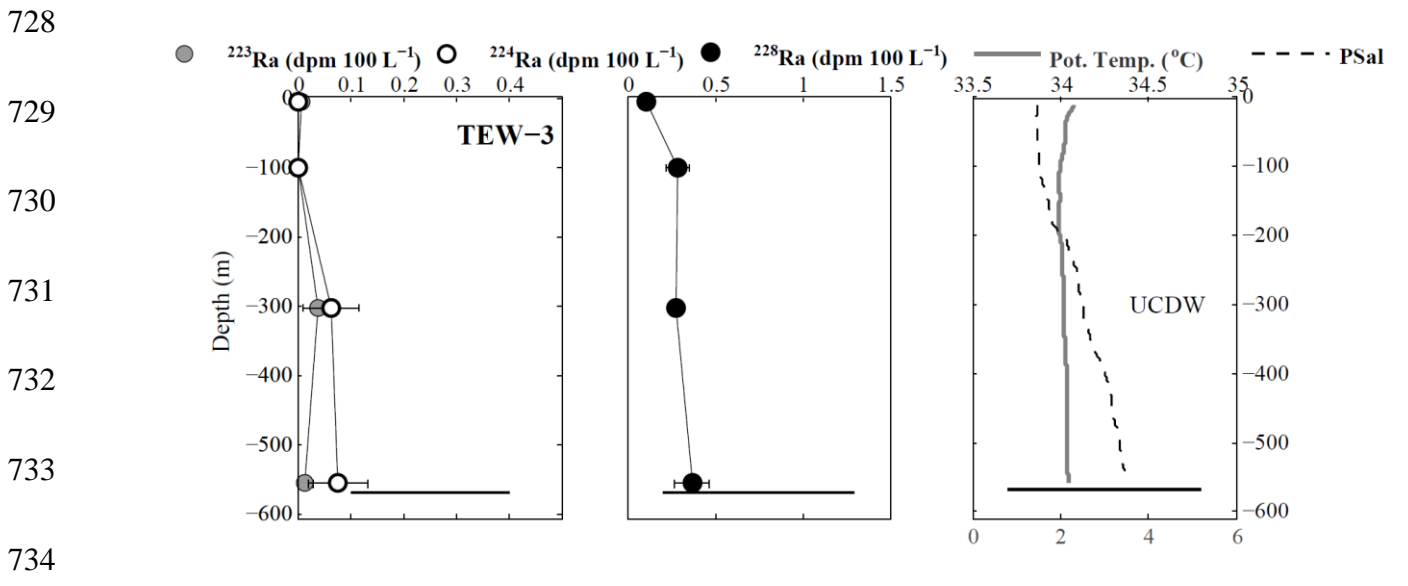
724 Fig. 4.

725

726



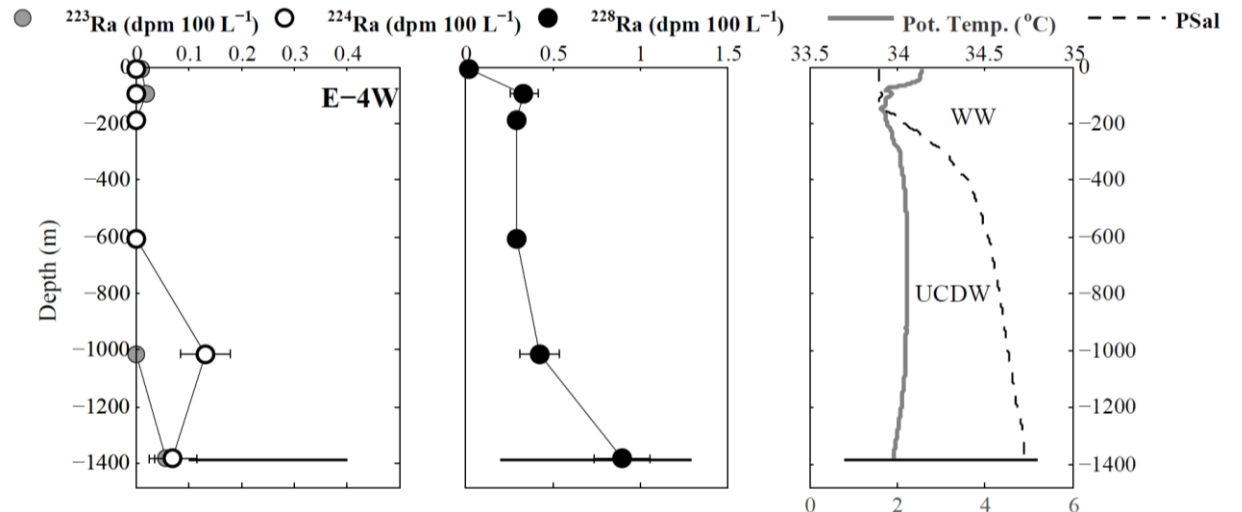
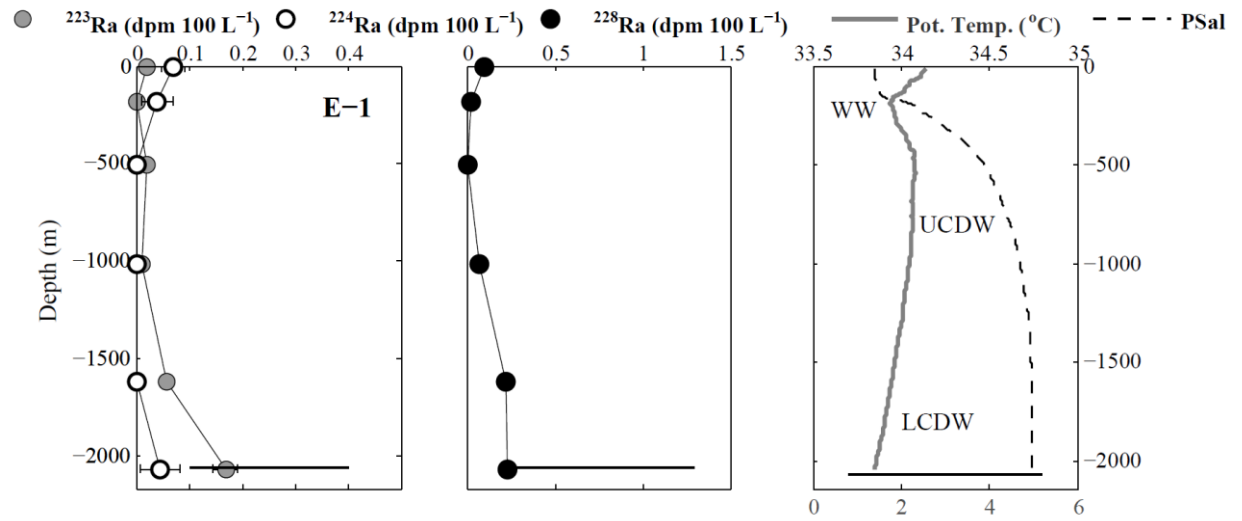
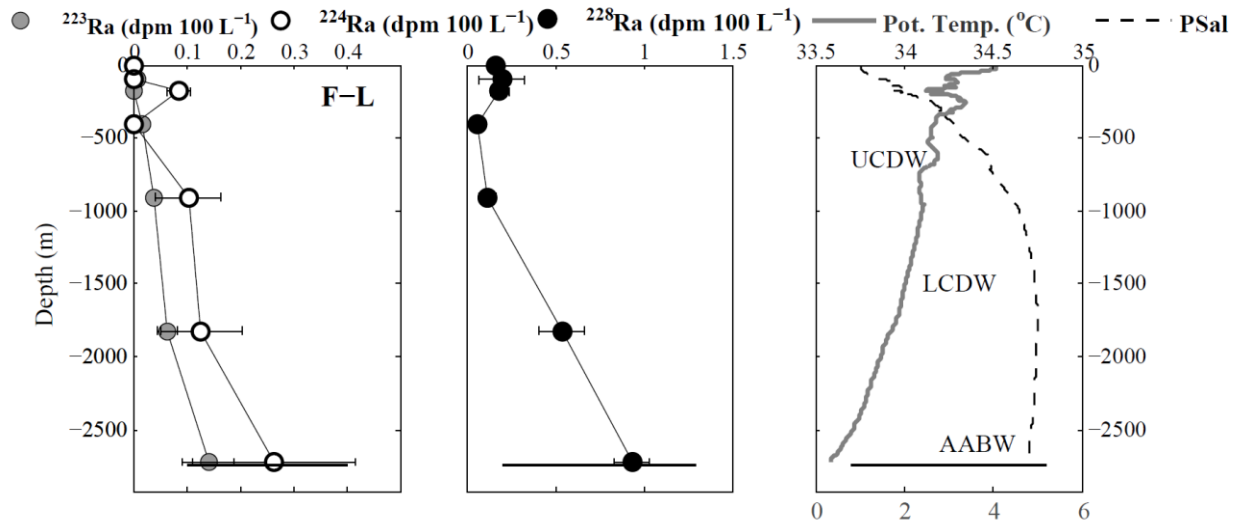
727 Fig. 5.



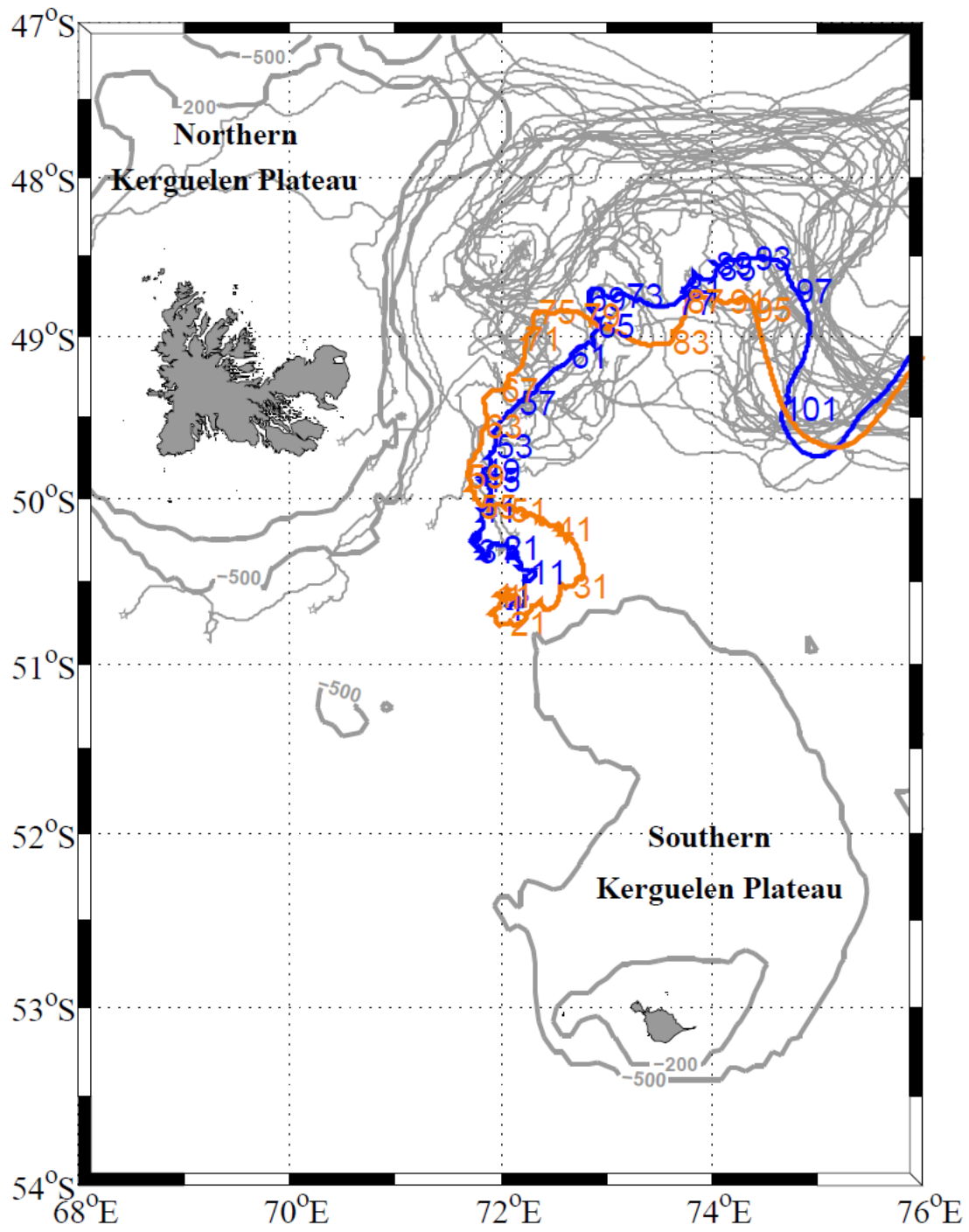
748 Fig. 6.

749

750



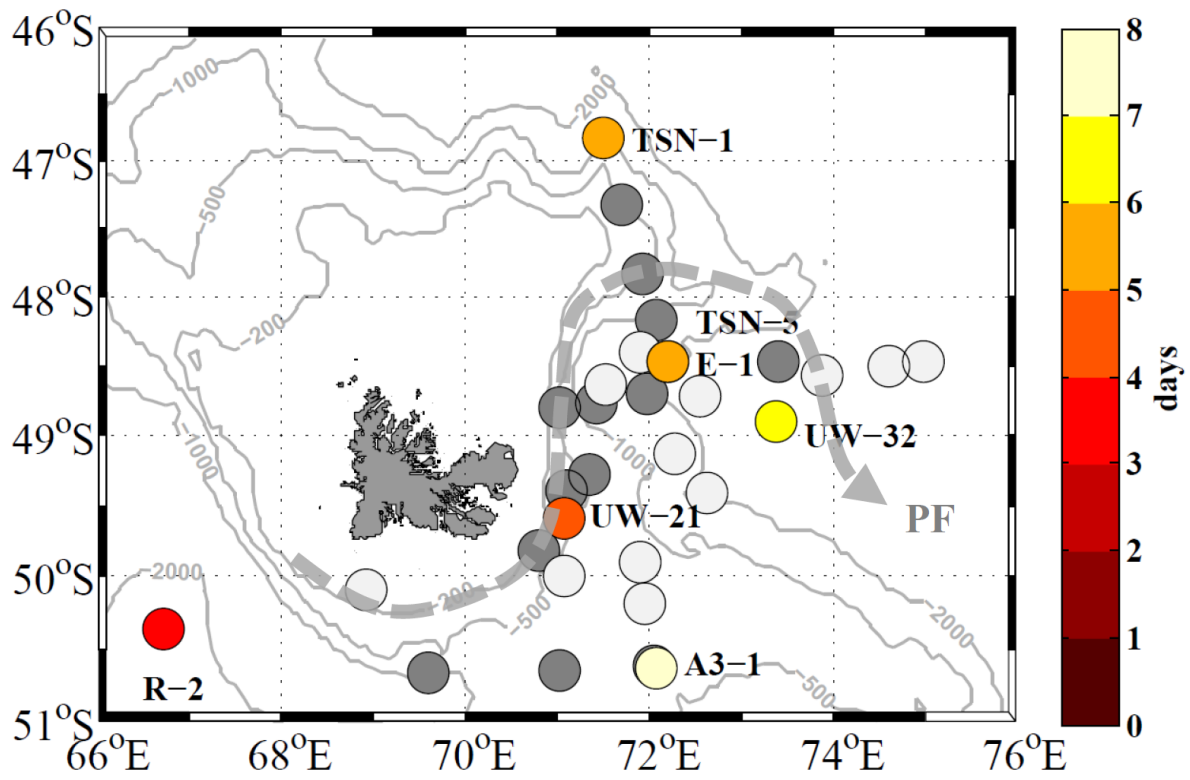
751 Fig. 7.



752

753

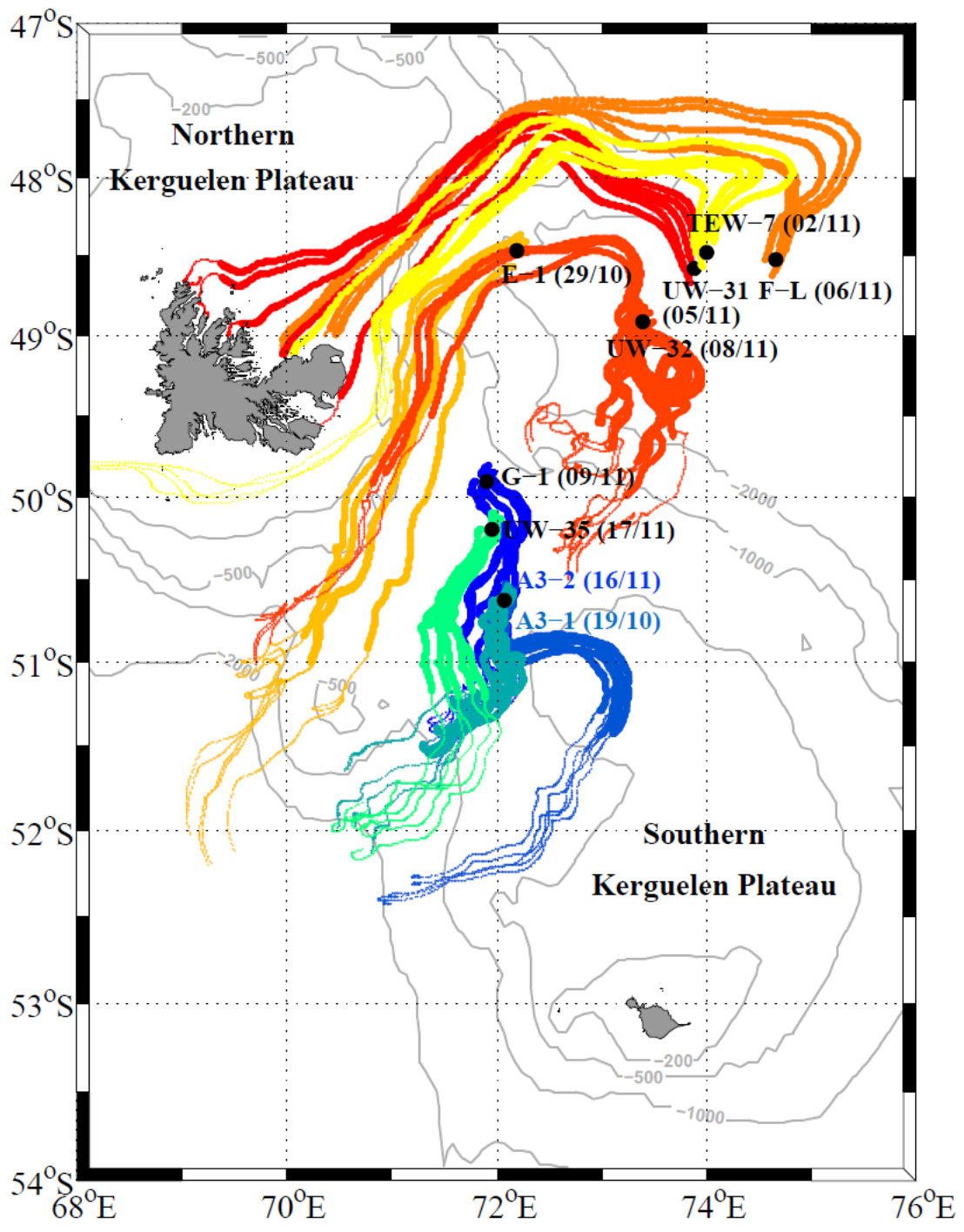
754 Fig. 8.



755

756

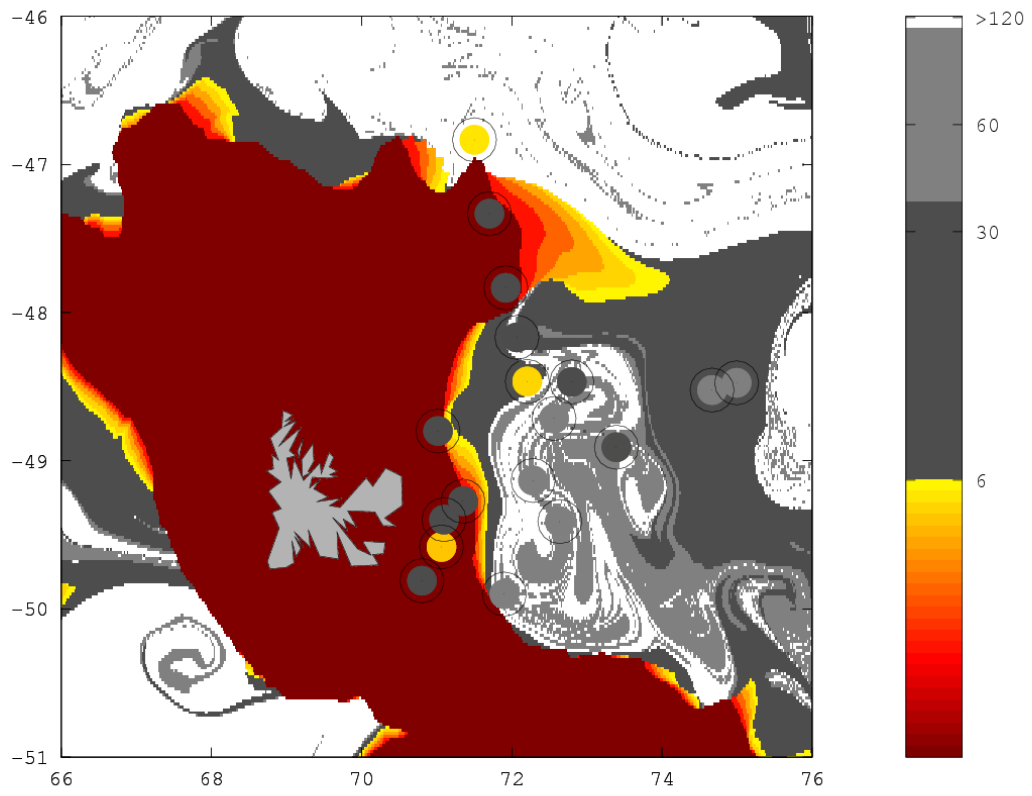
757 Fig. 9.



758

759

760 Fig. 10



761